



THE UNIVERSITY *of* EDINBURGH

Edinburgh Research Explorer

COMPLEMENT FACTOR B IS A DETERMINANT OF BOTH METABOLIC AND CARDIOVASCULAR FEATURES OF METABOLIC SYNDROME

Citation for published version:

Coan, P, Barrier, M, Alfazema, N, Carter, RN, Marion de Proce, S, Castro Dopico, X, Diaz, AG, Thomson, AJW, Jackson-Jones, L, Moyon, B, Webster, Z, Ross, D, Moss, J, Arends, MJ, Morton, NM & Aitman, TJ 2017, 'COMPLEMENT FACTOR B IS A DETERMINANT OF BOTH METABOLIC AND CARDIOVASCULAR FEATURES OF METABOLIC SYNDROME', *Hypertension*.
<https://doi.org/10.1161/HYPERTENSIONAHA.117.09242>

Digital Object Identifier (DOI):

[10.1161/HYPERTENSIONAHA.117.09242](https://doi.org/10.1161/HYPERTENSIONAHA.117.09242)

Link:

[Link to publication record in Edinburgh Research Explorer](#)

Document Version:

Publisher's PDF, also known as Version of record

Published In:

Hypertension

Publisher Rights Statement:

Hypertension is published on behalf of the American Heart Association, Inc., by Wolters Kluwer Health, Inc. This is an open access article under the terms of the Creative Commons Attribution License, which permits use, distribution, and reproduction in any medium, provided that the original work is properly cited

General rights

Copyright for the publications made accessible via the Edinburgh Research Explorer is retained by the author(s) and / or other copyright owners and it is a condition of accessing these publications that users recognise and abide by the legal requirements associated with these rights.

Take down policy

The University of Edinburgh has made every reasonable effort to ensure that Edinburgh Research Explorer content complies with UK legislation. If you believe that the public display of this file breaches copyright please contact openaccess@ed.ac.uk providing details, and we will remove access to the work immediately and investigate your claim.



Complement Factor B Is a Determinant of Both Metabolic and Cardiovascular Features of Metabolic Syndrome

Philip M. Coan, Marjorie Barrier,* Neza Alfazema,* Roderick N. Carter,
Sophie Marion de Procé, Xaquín C. Dopico, Ana Garcia Diaz, Adrian Thomson,
Lucy H. Jackson-Jones, Ben Moyon, Zoe Webster, David Ross, Julie Moss, Mark J. Arends,
Nicholas M. Morton, Timothy J. Aitman

Abstract—CFB (complement factor B) is elevated in adipose tissue and serum from patients with type 2 diabetes mellitus and cardiovascular disease, but the causal relationship to disease pathogenesis is unclear. Cfb is also elevated in adipose tissue and serum of the spontaneously hypertensive rat, a well-characterized model of metabolic syndrome. To establish the role of CFB in metabolic syndrome, we knocked out the *Cfb* gene in the spontaneously hypertensive rat. *Cfb*^{-/-} rats showed improved glucose tolerance and insulin sensitivity, redistribution of visceral to subcutaneous fat, increased adipocyte mitochondrial respiration, and marked changes in gene expression. *Cfb*^{-/-} rats also had lower blood pressure, increased ejection fraction and fractional shortening, and reduced left ventricular mass. These changes in metabolism and gene expression, in adipose tissue and left ventricle, suggest new adipose tissue-intrinsic and blood pressure-independent mechanisms for insulin resistance and cardiac hypertrophy in the spontaneously hypertensive rat. In silico analysis of the human *CFB* locus revealed 2 *cis*-regulated expression quantitative trait loci for *CFB* expression significantly associated with visceral fat, circulating triglycerides and hypertension in genome-wide association studies. Together, these data demonstrate a key role for *CFB* in the development of spontaneously hypertensive rat metabolic syndrome phenotypes and of related traits in humans and indicate the potential for CFB as a novel target for treatment of cardiometabolic disease. (*Hypertension*. 2017;70:00-00. DOI: 10.1161/HYPERTENSIONAHA.117.09242.) • [Online Data Supplement](#)

Key Words: adipose tissue ■ blood pressure ■ complement system proteins ■ glucose ■ hypertension

Metabolic syndrome (MetS) represents a complex clustering of cardiometabolic traits, including hypertension, insulin resistance, glucose intolerance, and dyslipidemia, all of which increase the risk of developing type 2 diabetes mellitus and cardiovascular disease.¹ Despite established environmental risk factors and genome-wide association study (GWAS) hits that link genetic variation to MetS constituents, the molecular and cellular events underlying its development remain incompletely understood.^{2,3}

Chronic low-grade inflammation and innate immune system overactivation are now recognized causes of type 2 diabetes mellitus and MetS.^{4,5} In particular, the alternative pathway (AP) has received attention for its potential causal role in cardiometabolic disease.⁶ AP activation requires CFB (complement factor B) to bind C3 to form C3B, which opsonises

pathogens and contributes to the formation of the membrane attack complex.⁶ Thus, CFB is fundamental to pathogen clearance and host cell apoptosis. However, increased circulating CFB has been found in patients with type 2 diabetes mellitus,⁷ and expression of adipose tissue CFB correlates significantly with fasting glucose and circulating lipids.⁸ Elevated circulating CFB has also been found to increase the risk of endothelial dysfunction⁹ and coronary heart disease.¹⁰

Because of the complex genetic basis of human MetS, the spontaneously hypertensive rat (SHR), which exhibits hypertension, insulin resistance, and dyslipidemia, has been extensively studied as a MetS model.^{11–13}

Multiple studies have identified SHR genes associated with features of MetS, many of which show conserved pathologies in humans.^{14–17}

Received February 13, 2017; first decision February 22, 2017; revision accepted June 2, 2017.

From the Centre for Genomic and Experimental Medicine, MRC Institute for Genetics and Molecular Medicine, Edinburgh, United Kingdom (P.M.C., M.B., N.A., S.M.P., X.C.D., D.R., J.M., T.J.A.); British Heart Foundation Centre for Cardiovascular Science, Queen's Medical Research Institute (P.M.C., M.B., N.A., R.N.C., A.T., L.H.J.-J., N.M.M., T.J.A.) and Royal (Dick) School of Veterinary Studies (X.C.D.), University of Edinburgh, United Kingdom; Department of Medicine (A.G.D., T.J.A.) and Embryonic Stem Cell and Transgenics Facility, MRC Clinical Sciences Centre (B.M., Z.W.), Imperial College London, United Kingdom; and Division of Pathology, Centre for Comparative Pathology, Cancer Research UK Edinburgh Centre, United Kingdom (M.J.A.).

*M.B. and N.A. contributed equally to this study.

The online-only Data Supplement is available with this article at <http://hyper.ahajournals.org/lookup/suppl/doi:10.1161/HYPERTENSIONAHA.117.09242/-/DC1>.

Correspondence to Philip M. Coan, Centre for Genomic and Experimental Medicine, MRC Institute for Genetics and Molecular Medicine, Edinburgh, EH4 2XU, United Kingdom. E-mail p.m.coan.02@cantab.net

© 2017 The Authors. *Hypertension* is published on behalf of the American Heart Association, Inc., by Wolters Kluwer Health, Inc. This is an open access article under the terms of the [Creative Commons Attribution](#) License, which permits use, distribution, and reproduction in any medium, provided that the original work is properly cited.

Hypertension is available at <http://hyper.ahajournals.org>

DOI: 10.1161/HYPERTENSIONAHA.117.09242

The rat *Cfb* gene resides within the major histocompatibility region on chromosome 20p12.¹⁸ In SHR, this region has been demonstrated to be important in blood pressure regulation,¹⁹ serum cholesterol, adiposity, and glucose tolerance.^{20,21} In this study, we knocked out *Cfb* in SHR to test the hypothesis that *Cfb* is necessary for the full expression of cardiometabolic pathophysiological traits in this model of MetS.

Methods

Detailed methods are available in the [online-only Data Supplement](#).

Rats

Cfb^{-/-} rats were generated using SHR/NCrl rats (Charles River, Margate, United Kingdom), by microinjecting Zinc-finger nuclease (ZFN) mRNA (Sigma), targeted to exon 6 of *Cfb* (target sequence: CCCCT CGGGCTCCATGaatatcTACATGGTGCTGGATG), into 1-cell stage SHR/NCrl embryos that were implanted into pseudopregnant rats. Heterozygous progeny, from a founder harboring a 19-base pair deletion in *Cfb*, were intercrossed to homozygosity. A search for off-target events, conducted by whole genome sequencing confirmed the 19-base pair deletion. Six additional putative mutations, analyzed by Sanger Sequencing, were determined to be false positives (Table S1). Rats were housed with free access to food and water. All procedures were performed in accordance with UK Home Office regulations.

Statistics

Unpaired *t* test or 2-way ANOVA (Minitab Express) were used to assess differences between genotype and treatment. All results are mean±SEM. *P*<0.05 was considered significant.

Results

Generation of a *Cfb* Knockout Rat

Using data from a quantitative trait transcript analysis of recombinant inbred strains derived from a SHR×Brown Norway (BN-Lx/Cub) cross,²² we identified *Cfb* transcript levels as uniquely and strongly correlated significantly across the recombinant inbred strains for metabolically relevant traits (glucose uptake in isolated adipocytes, $r^2=-0.65$, $P_{(adj)}=0.0003$; basal lipogenesis in epididymal fat, $r^2=-0.64$, $P_{(adj)}=0.0002$; serum high-density lipoprotein cholesterol, $r^2=-0.64$, $P_{(adj)}=0.0005$) and significantly differentially expressed in adipose tissue between parental strains (SHR versus Brown Norway, 1.47-fold $P_{(adj)}<0.05$). Overexpression in SHR adipose tissue was confirmed by quantitative polymerase chain reaction by comparing a further insulin sensitive/normotensive Wistar Kyoto strain (WKY/NCrl; Figure S1A). *Cfb* was also overexpressed in SHR left ventricle (LV), but not liver, compared with WKY (Figure S1A). *Cfb* overexpression in SHR was associated with increased AP activity compared with WKY (Figure S1B). Analysis of the *Cfb* gene and its adjacent region revealed 14 variants unique to SHR, not present in Brown Norway or WKY; 2 variants reside upstream of the transcription start site (Figure S1C). To investigate the potential causative role of *Cfb* in the cardiometabolic traits of SHR, a 19-base pair deletion in exon 6 of the *Cfb* gene in the SHR germline was made using ZFNs (Figure S1D). Abolition of *Cfb* expression was confirmed by quantitative polymerase chain reaction and immunoblot (Figure S1E), and loss of Cfb function was confirmed by ablation of serum AP activity (Figure S1F).

Glucose Homeostasis

To test whether *Cfb* ablation affected glucose homeostasis in SHR, oral glucose tolerance and insulin sensitivity (IVITT

[intravenous insulin tolerance test]) were assessed. Fasting plasma glucose concentration in *Cfb*^{-/-} was significantly lower than SHR (Figure 1A; SHR, 4.62 ± 0.10 versus *Cfb*^{-/-}, 4.25 ± 0.09 ; $P=0.013$). Throughout the oral glucose tolerance, blood glucose remained lower, and area under the glucose curve was significantly reduced in *Cfb*^{-/-} compared with SHR; insulin concentrations were similar in both groups (Figure 1A and 1B). Together with the G:I ratio (ratio of area under the curve of plasma glucose concentration to area under the curve of plasma insulin concentration; Figure 1C), this indicated an improvement in insulin sensitivity, further demonstrated in IVITTs by a significant 48% increase in insulin-stimulated glucose disposal (K_{ITT}) in *Cfb*^{-/-} compared with SHR (Figure 1D).

Adipose Tissue Function

To determine whether *Cfb* affects adipose function, as suggested by our previous quantitative trait transcript analysis and metabolic phenotyping, we measured adipose tissue depot masses. Relative wet masses of visceral (epididymal adipose tissue [EAT]; mesenteric adipose tissue [MAT]; and retroperitoneal adipose tissue) and brown fat (brown adipose tissue [BAT]) were significantly reduced in *Cfb*^{-/-} rats compared with SHR, despite similar total body mass (269 ± 20 versus 265 ± 31 g; $P>0.05$; Figure 2A); however, *Cfb*^{-/-} had significantly more relative subcutaneous fat (SAT; Figure 2A). Overall, total fat mass was similar (SHR, 42.9 ± 1.4 versus *Cfb*^{-/-}, 42.8 ± 1.4 g/kg; $P>0.05$). Stereological analysis of EAT showed that *Cfb*^{-/-} had significantly fewer, similar-sized adipocytes than SHR (SHR, 4.06 ± 0.21 versus *Cfb*^{-/-}, $4.13\pm0.32\times10^5 \mu\text{m}^3$; $P>0.05$; Figure 2B). Further, serum analysis of circulating lipids and adipokines demonstrated significant decreases in levels of cholesterol, triglycerides, and high molecular-weight adiponectin (-48%), in *Cfb*^{-/-} compared with SHR; however, circulating total adiponectin and leptin were similar (Table S4).

Given the varied metabolic contributions of different fat depots found in the *Cfb*^{-/-} rat, we analyzed transcript abundance for markers of oxidation (*Cpt1* and *Aco1*), beigeing (*Ucp1* and *Pgc1a*), insulin sensitivity (*Slc2a4*), lipid metabolism (fatty acid synthase [*Fasn*]), and adipokines (*Adipoq* and *Lep*). In EAT, *Pgc1a*, *Cpt1*, *Aco1*, and *Slc2a4* were significantly increased in *Cfb*^{-/-} compared with SHR (Figure 2C). In SAT, *Aco1*, *Ucp1*, *Fasn*, and *Adipoq* were significantly elevated, whereas *Pgc1a* was reduced, in *Cfb*^{-/-} compared with SHR (Figure 2D). In BAT, *Pgc1a* and *Slc2a4* were significantly increased in *Cfb*^{-/-} compared with SHR, whereas *Ucp1* and *Fasn* were significantly decreased (Figure 2E). *Lep* was significantly reduced in all *Cfb*^{-/-} depots compared with SHR (Figure 2C through 2E).

To determine whether transcript changes were associated with altered adipose tissue respiration, we analyzed epididymal adipocyte metabolic rate. Maximal and basal respiratory rates were significantly greater in *Cfb*^{-/-} than in SHR, $+1.64$, and $+1.96$ -fold, respectively (Figure 2; Figure S2A). Further, reserve capacity and leak respiration were both significantly increased (Figure S2B and S2C). However, ATP-linked respiration and ATP-generation efficiency were similar (Figure S2D through S2E). CoxIV protein abundance—a mitochondrial marker—was similar in both *Cfb*^{-/-} and SHR (Figure S2F).

There were no differences in body temperature or activity associated with *Cfb* deletion (Figure S3A and S3B).

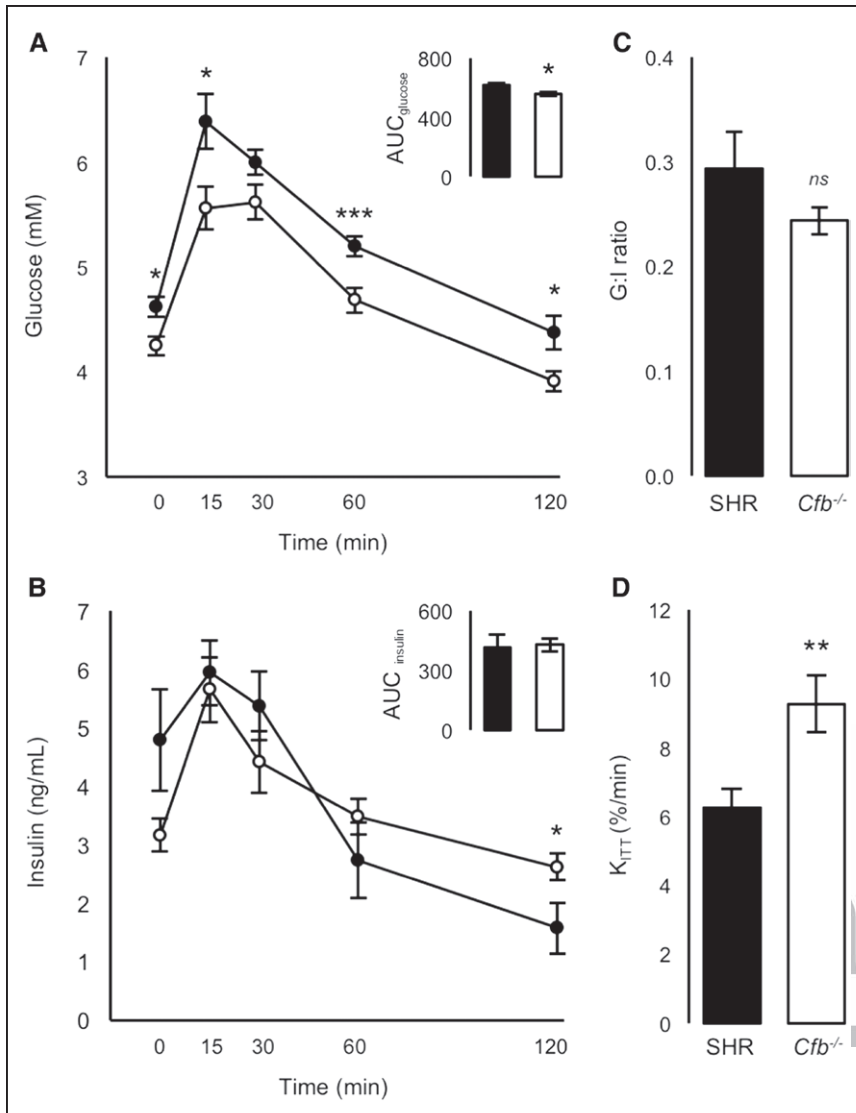


Figure 1. Glucose homeostasis. **A**, Glucose concentration curve during oral glucose tolerance (OGTT; inset, area under the curve, area under the curve (AUC), glucose. **B**, Plasma insulin concentration curve of OGTT (inset; area under the curve insulin). **C**, G:I ratio, (AUC_{glucose}:AUC_{insulin}). **D**, Insulin-stimulated glucose clearance (K_{ITT}). Spontaneously hypertensive rat (SHR), filled bars/circles, *Cfb*^{-/-}, open bars/circles. **P*<0.05, ***P*<0.01, ****P*<0.005. G:I indicates ratio of area under the curve of plasma glucose concentration to area under the curve of plasma insulin concentration.

Cardiovascular Analyses

Cfb deletion reduced relative LV mass and cardiomyocyte diameter by 10% compared with SHR; however, relative heart weight was similar between genotypes (Figure 3A and 3B; Figure S4A and S4B). Telemetrically measured systolic and diastolic blood pressures were significantly lower ($-\Delta 7$ mm Hg) in *Cfb*^{-/-} than in SHR, and although heart rate was similar, rate pressure product was significantly reduced (Figure 3C and 3D; Figure S4C through S4F). Serum aldosterone and transcripts for renal renin and hepatic angiotensinogen were all significantly reduced in *Cfb*^{-/-} rats (Table S4, Figure S5A and S5B).

Early structural and functional changes in the heart were investigated using echocardiography. We confirmed that relative LV mass was significantly reduced in *Cfb*^{-/-} compared with SHR; however, at this stage, LV wall thickness was not significantly different (Table S5). Functionally fractional shortening and ejection fraction were significantly increased in *Cfb*^{-/-} LV compared with SHR (Table S5). Given the similar heart rate and stroke volume, cardiac output was not significantly different (Table S5).

An acute hypertrophic challenge designed to investigate whether *Cfb* deletion conferred protection from cardiac stress,

independent of blood pressure, showed that the rate pressure product was significantly reduced in *Cfb*^{-/-} hearts in the 24 hours after isoproterenol treatment (Figure 3E and 3F; Figure S6A). Isoproterenol increased relative heart and LV mass similarly (Figure S6B and S6C). Transcripts related to cardiac hypertrophy were investigated in LV from isoproterenol and saline-treated rats. In saline-treated *Cfb*^{-/-} rats, *Nppa*, *Actc1*, and *Camk2d* were significantly increased compared with SHR (Figure 4A, 4C, and 4E); whereas *Nppb* was significantly decreased (Figure 4B). In isoproterenol-treated rats, *Nppb* increased marginally in *Cfb*^{-/-} rats compared with SHR (Figure 4B). *Acta1* in isoproterenol-treated *Cfb*^{-/-} rats was similar to both saline-treatment groups (Figure 4F). The ratio of *Actc1*:*Acta1* was significantly greater in *Cfb*^{-/-} compared with SHR, in saline-treated (317 ± 43 versus 138 ± 18 ; *P*=0.05) and isoproterenol-treated rats (256 ± 37 versus 53 ± 9 ; *P*<0.005). *Myh6* and *Myh7* expression was similar between genotypes (Figure 4D; Figure S7).

Serum Markers of Inflammation

Given the function of *Cfb* in inflammatory responses, we determined the effect of *Cfb*^{-/-} on Th-1 mediated inflammation by quantifying serum concentrations of cytokines (IL-2,

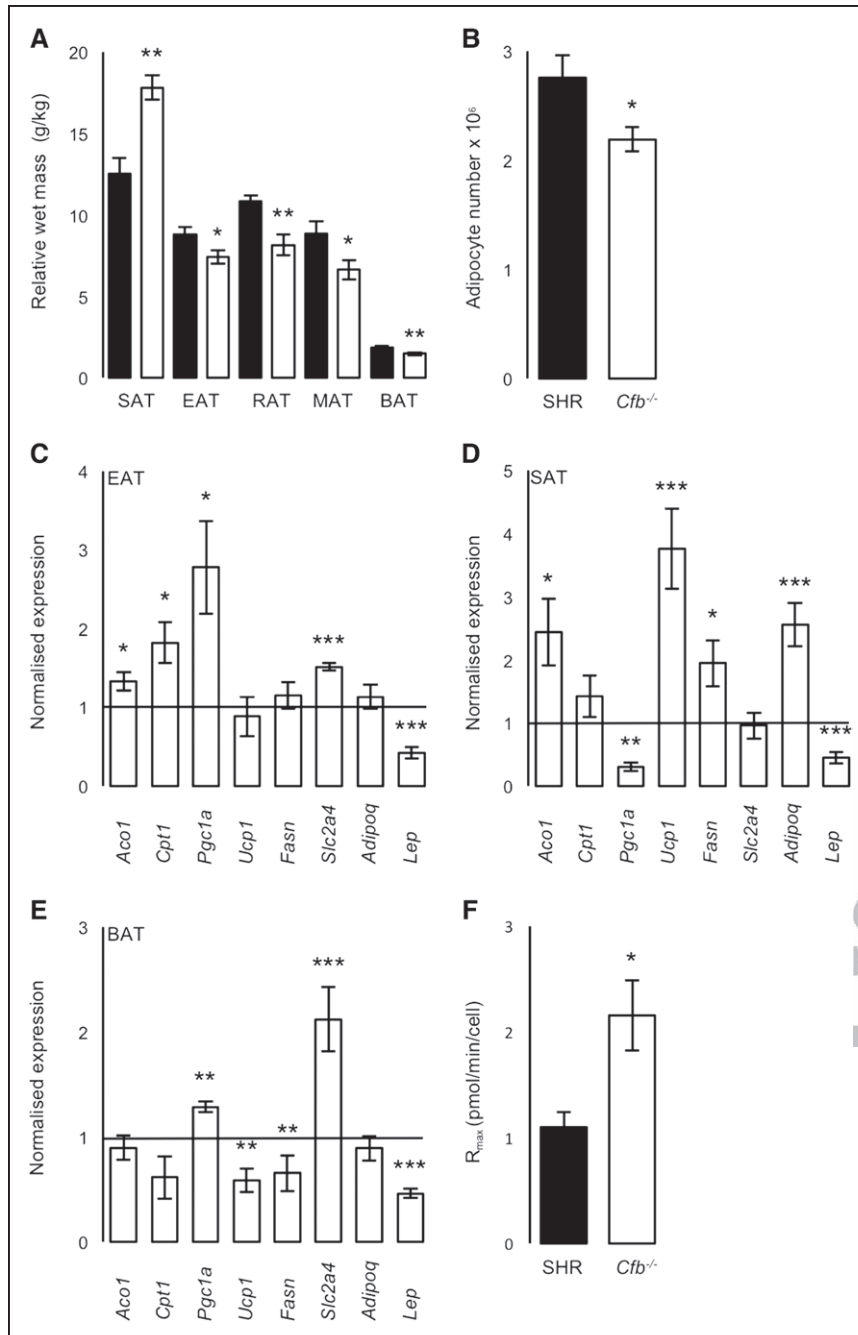


Figure 2. Adipose tissue and adipocyte morphometry, gene expression, and respiratory capacity. **A**, Adipose tissue wet masses, including subcutaneous (SAT), epididymal (EAT), retroperitoneal (RAT), mesenteric (MAT), and brown (BAT; $n=6$ per group). **B**, Epididymal mean cell number ($n=6$ per group). **C**, EAT, **D** SAT, **E** BAT gene expression levels in *Cfb*^{-/-}, normalized to *Actb* ($n=5$ per group). **F**, Maximal respiratory rates in primary epididymal adipocytes. Spontaneously hypertensive rat (SHR), filled bars, *Cfb*^{-/-}, and open bars. *Aco1* indicates aconitase 1; *Adipoq*, adiponectin; *Cpt1*, carnitine palmitoyltransferase 1; *Fasn*, fatty acid synthetase; normalized expression, gene of interest normalized to β -actin; *Lep*, leptin; *Pgc1a*, peroxisome proliferator-activated receptor gamma coactivator 1 alpha *Slc2a4*, solute carrier family 2 member 4; and *Ucp1*, uncoupling protein 1. * $P<0.05$, ** $P<0.01$, *** $P<0.005$.

Il-6, Il-10, granulocyte macrophage colony stimulating factor, $\text{Ifn-}\gamma$, and $\text{Tnf}\alpha$). We found significant decreases in serum concentrations of Il-10 and $\text{Ifn-}\gamma$ in *Cfb*^{-/-} rats compared with SHR. In addition, whereas Il-6 and $\text{Tnf}\alpha$ were detected in SHR, the cytokines were undetectable in sera from *Cfb*^{-/-} rats. Granulocyte macrophage colony stimulating factor was similar in both groups, and in neither group was Il-2 detected (Table S4).

Analysis of GWAS Hits and *cis*-Expression QTLs at the Human *CFB* Locus

To determine whether genetic variants near *CFB* are associated with metabolic and cardiovascular disorders relevant to MetS (Table S3), we mined the NHGRI GWAS catalog

(National Human Genome Research Institute) and located 18 single-nucleotide polymorphisms (SNPs) associated with cardiometabolic traits ≤ 1 Mb from *CFB* (Figure 5; Table S6). Six SNPs were found to be associated with type 2 diabetes mellitus, MetS, or visceral fat. Six further SNPs were related to circulating lipids. The remaining SNPs were associated with coronary heart disease and hypertension (Table S6).

We also investigated whether variants at the *CFB* locus are associated with *CFB* expression by mining GTEx datasets (the Genotype-Tissue Expression project) for *CFB* *cis*-expression quantitative trait loci (QTLs). Fifty-three SNPs were associated with *CFB* expression in 4 tissues (Figure 5; Table S7). One SNP, rs76846904, close to the *HLA-DRB5* gene, is highly correlated with *CFB* gene expression in subcutaneous

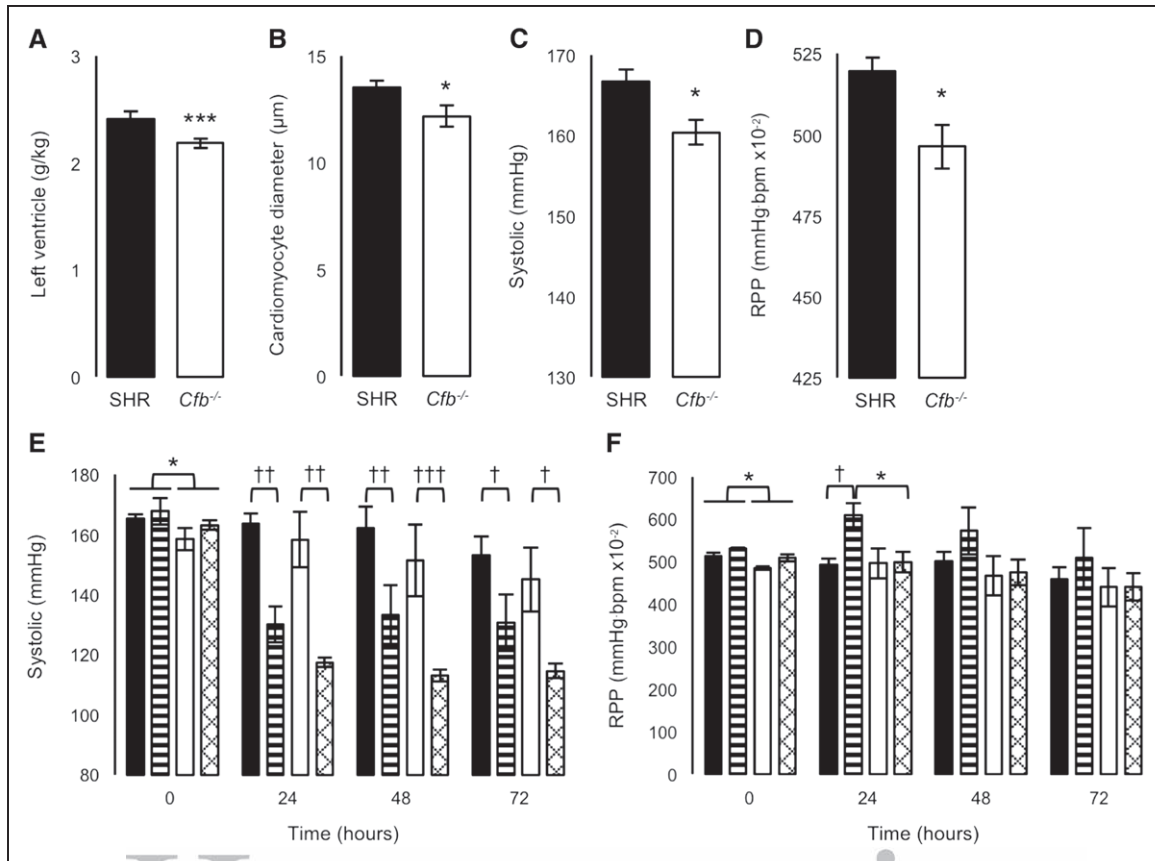


Figure 3. Left ventricle morphometry, blood pressure, and rate pressure product before and after 72-h infusion of isoproterenol or saline. **A**, Left ventricle wet mass and **(B)** mean left ventricular cardiomyocyte diameter. **C**, baseline mean systolic blood pressure and **(D)** rate pressure product recorded telemetrically. **E**, Mean systolic blood pressure and **(F)** rate pressure product recorded telemetrically during infusion of isoproterenol or saline. Black-filled bars, spontaneously hypertensive rat (SHR), saline-treated; stripe-filled bars, SHR, isoproterenol-treated; white-filled bars, *Cfb*^{-/-}, saline-treated; hatch-filled bars, *Cfb*^{-/-}, isoproterenol-treated. Differences in genotype **P*<0.05, ****P*<0.0005 or treatment †*P*<0.05, ††*P*<0.005, †††*P*<0.0005.

adipose tissue (effect size, 0.78; *P*=0.000015) and within 100 kb of GWAS hits for visceral adiposity, serum cholesterol, and coronary heart disease.

The influence of the 18 GWAS SNPs, or any of their proxies (a total of 280 SNPs), on gene expression across 9 tissues was investigated using the GTEx Portal. Four SNPs were significantly associated (false discovery rate<0.05) with *CFB* expression in tissues of interest (Figure 5; Tables S6 and S7). Two SNPs, correlating with *CFB* expression in “adipose subcutaneous” and “artery aorta”, respectively, are proxies for rs13196329 and rs2247056, which are associated with visceral fat and triglycerides in the GWAS catalog (Table, Figure 5). Two further SNPs were significantly associated with increased *CFB* expression in “heart LV” and correspond to the same SNP (rs805303) that is associated with increased systolic and diastolic blood pressure and hypertension in the GWAS catalog (Table; Figure 5).

Discussion

We tested the hypothesis that *Cfb* is necessary for the full expression of cardiometabolic pathophysiological traits in the SHR model of MetS. Through ZFN-mediated gene knockout, we showed that the *Cfb*-deficient (*Cfb*^{-/-}) SHR has improved glucose tolerance and insulin sensitivity, along with favorable adipose tissue distribution, adipose oxidative capacity,

and reduced circulating lipids and proinflammatory cytokines compared with parental SHR. Further, *Cfb*^{-/-} rats had reduced blood pressure that was associated with increased ejection fraction and fractional shortening and reduced LV mass. The human *CFB* locus—a gene-rich region within the major histocompatibility complex—contains several GWAS hits for cardiometabolic traits, including coronary heart disease, blood pressure, MetS, type 2 diabetes mellitus, serum lipids, and visceral fat. These colocalize with *cis*-expression QTLs associated with expression of *CFB* in subcutaneous adipose tissue and other tissues, indicating that variation in *CFB* expression may underlie, in part, the GWAS hits at this locus.

Glucose intolerance, insulin resistance, visceral adiposity, and dyslipidemia are the key metabolic features of MetS that increase the risk of type 2 diabetes mellitus.²³ In our study, *Cfb*^{-/-} rats had reduced visceral but increased subcutaneous fat. To investigate potential molecular changes associated with favorably altered fat distribution and ameliorated glucose homeostasis in *Cfb*^{-/-} rats, we investigated transcripts central to adipose tissue metabolism. Reduced EAT mass in *Cfb*^{-/-} rats was because of reduced adipocyte number rather than altered adipocyte volume. *Pgc1a*, *Cpt1*, and *Acol* were upregulated in *Cfb*^{-/-} rats, suggestive of increased adipocyte oxidative phosphorylation, which we confirmed by Seahorse

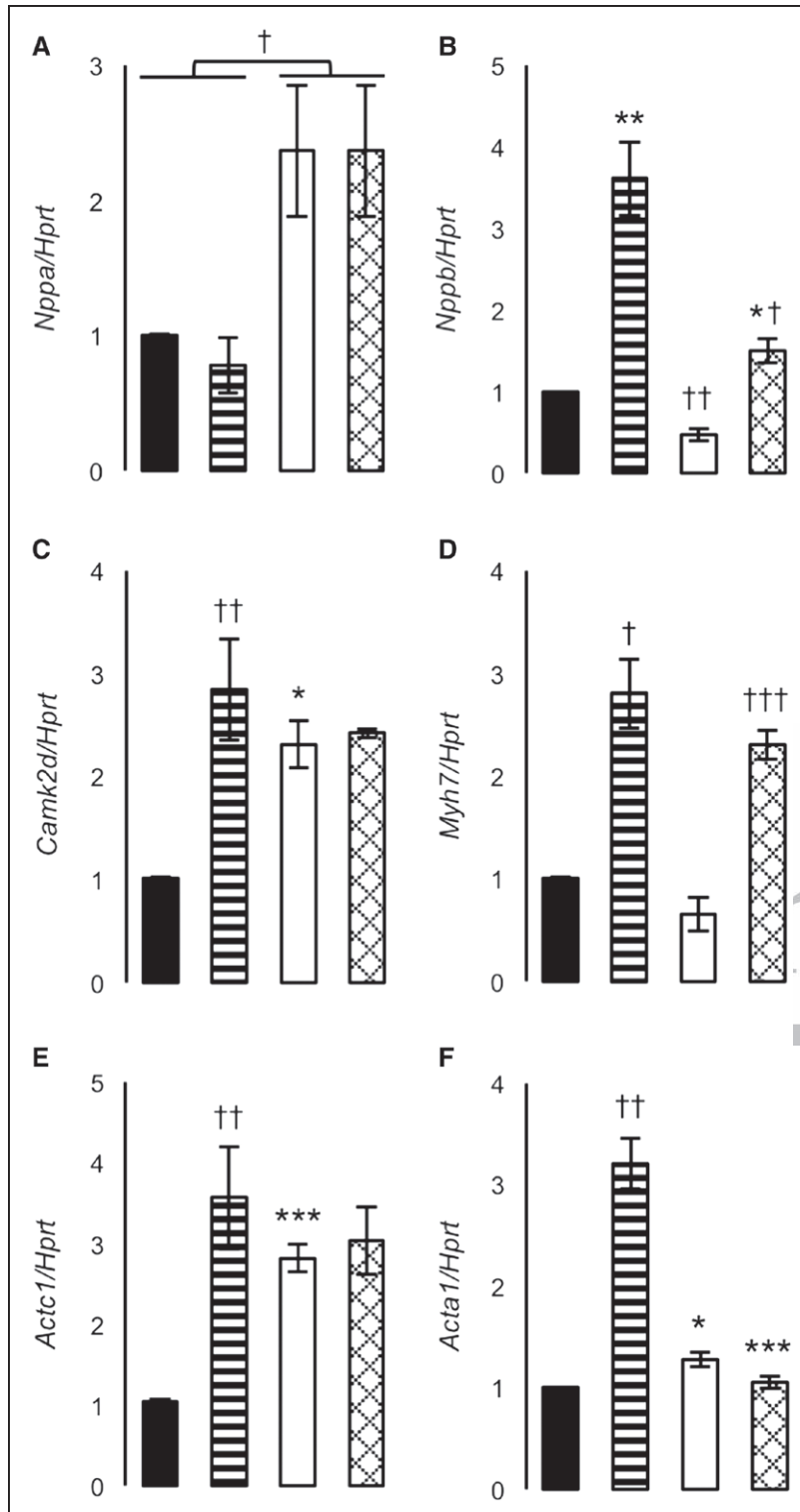


Figure 4. Gene expression levels in left ventricles after 72-h isoproterenol or saline treatment. **A**, *Nppa*, natriuretic peptide a, **(B)** *Nppb*, brain natriuretic peptide, **(C)** *Camk2d*, calcium/calmodulin dependent protein kinase II delta *Myh6*, **(D)** *Myh7*, myosin heavy polypeptide 7, **(E)** *Actc1*, α -cardiac actin, **(F)** *Acta1*, α -skeletal actin. Black-filled bars, SHR, saline-treated; stripe-filled bars, spontaneously hypertensive rat (SHR), isoproterenol-treated; white-filled bars, *Cfb*^{-/-}, saline-treated; hatch-filled bars, *Cfb*^{-/-}, isoproterenol-treated. Differences in genotype **P*<0.05, ***P*<0.005, ****P*<0.0005 or treatment †*P*<0.05, ††*P*<0.005, †††*P*<0.0005.

analysis. *Cfb*^{-/-} rats exhibited a marked increase in basal and maximal respiration and had a 2-fold increased reserve respiratory capacity. Taken together with the reduction in adipocyte number, the data suggest that the elevation of mitochondrial respiratory capacity may provide an adipose tissue-intrinsic mechanism for reduced fat accumulation in *Cfb*^{-/-} EAT. In SAT, increased mass in *Cfb*^{-/-} rats was associated with increased *Fasn* and reduced *Pgc1a* expression, consistent

with the function of *Fasn* as an insulin-sensitive fatty acid synthase, the role of *Pgc1a* in stimulating fatty acid oxidation, and the known upregulation of *FASN* in human obesity and type 2 diabetes mellitus.²⁴ These changes seemed to override the increases in *Aco1* and *Ucp1* expression observed in *Cfb*^{-/-} rats, which would be expected to reduce adipocyte mass through increased trichloroacetic acid cycle activity and thermogenesis. The redistribution of visceral to subcutaneous

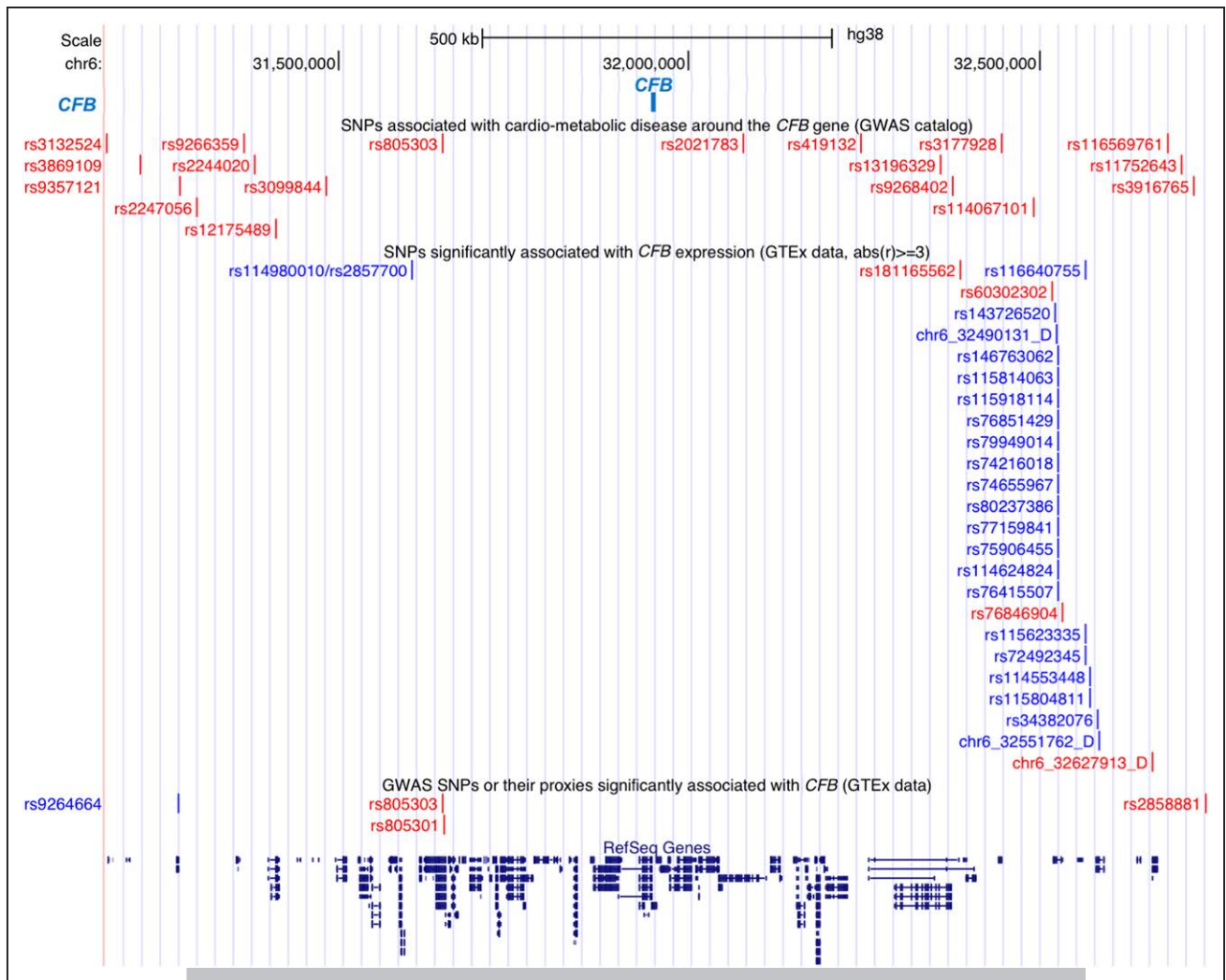


Figure 5. Cardiometabolic genome-wide association study (GWAS) hits and *cis*-eQTLs (quantitative trait loci) located in the human complement factor B (*CFB*) locus. Eighteen relevant cardiometabolic single-nucleotide polymorphisms (SNPs) located <1 Mb from the boundaries of the human *CFB* gene (upper; red). Twenty-six SNPs were retrieved from the GTEx Portal that were found to be significantly associated with *CFB* expression ($P < 0.05$), blue SNPs are associated with a significant negative effect, whereas red SNPs are associated with a significant positive effect. Four SNPs (with 1 overlapping) were determined to be correlated to both *CFB* expression, as well as being GWAS hits for relevant cardiometabolic traits (lower; red/blue). See Table S8 for a list of genes located in the *CFB* locus.

fat marked changes in gene expression, and adipose respiratory capacity are likely to be the key to improvements in whole-body glucose homeostasis and metabolic function in *Cfb*^{-/-} rats. Reduced BAT mass in *Cfb*^{-/-} rats was associated with increased *Pgcl1a* and *Slc2a4* and decreased *Ucp1* and *FASN* expression. This fat reduction may be consistent with increased *Pgcl1a* driving lipolysis although inhibiting fatty acid synthesis; however, further experiments in *Cfb*^{-/-} rats will be required to understand the BAT energy-substrate balance resulting from *Cfb* deficiency.

To further investigate altered adipose function in the *Cfb*^{-/-} rat, we quantified *Lep* and *Adipoq* transcripts in EAT, SAT, and BAT. Although adipose *Lep* expression was reduced, circulating leptin was comparable in *Cfb*^{-/-} and SHR. Although incompletely explained here, this could be accounted for by differences in post-translational processing and release, or peripheral metabolism, of leptin. Despite increased *Adipoq* expression in SAT alone, circulating high molecular-weight adiponectin

was reduced in *Cfb*^{-/-} rats. Conversely, high molecular-weight adiponectin in humans is lower in obese, insulin-resistant compared with lean, insulin-sensitive individuals.²⁵ However, adiponectin deficiency in mice has been shown to have no effect on glucose homeostasis on a normal diet.^{26,27} Further, infusion of adiponectin in high-fat fed SHR only marginally reduced insulin levels without affecting energy expenditure or hypertension.²⁸ Taken together with the observed metabolic improvements, this suggests other mechanisms, besides adiponectin, drive insulin sensitization in the *Cfb*^{-/-} rat.

We also tested the hypothesis that deletion of *Cfb* in SHR would affect the expression of SHR cardiovascular phenotypes. In this study, we showed that *Cfb*^{-/-} rats had reduced systolic and diastolic blood pressure, reduced LV mass and cardiomyocyte diameter, and an abrogated isoproterenol-induced increase in rate pressure product. These alterations represent a marked amelioration in several of the key cardiovascular features of MetS manifested in SHR.

Table. *cis*-eQTL SNPs Significantly Correlated With *CFB* Gene Expression and GWAS Hits

SNP identifier	Distance From TSS	Nominal P Value	P Value (FDR)*	Slope†	Tissue	Proxy/GWAS Hit
rs805303	−297084	0.0020	0.0489	0.226	heart left ventricle	GWAS hit
rs805301	−295329	0.0020	0.0489	0.226	heart left ventricle	proxy to rs805303
rs9264664	−674223	0.0012	0.0263	−0.224	artery aorta	proxy to rs2247056
rs2858881	790395	0.0028	0.0408	0.387	adipose subcutaneous	proxy to rs13196329

CFB indicates Complement factor b; FDR, false discovery rate; GWAS, genome-wide association study; QTL, quantitative trait locus; SNP, single-nucleotide polymorphisms; and TSS, transcription start site.

*P value (FDR), P value after adjustment for false discovery rate.

†Slope of the correlation curve between SNP and *CFB* expression.

The reduction in blood pressure was associated with reductions in renin–angiotensin system components, suggesting that *Cfb* may have a direct effect, yet unexplained, on this system, mediating blood pressure and subsequently LV mass. Although *Cfb* deletion leads to lower blood pressure in SHR, our experiments do not distinguish whether *Cfb* is responsible for increasing above or maintaining basal blood pressure. Further detailed experiments are required to distinguish these 2 possible mechanisms.

To gain further insight into the molecular changes caused by *Cfb* deficiency in the heart, we investigated the effect of *Cfb* deletion on cardiomyogenic genes (ie, *Nppa*, *Nppb*, *Myh6*, *Myh7*, *Acta1*, and *Camk2d*), which are activated in response to stress.²⁹ Our study showed that despite reduced LV mass, *Camk2d* expression was significantly increased in saline-treated *Cfb*^{−/−}. CaMKII (calcium/calmodulin-dependent protein kinase type 2) is proposed to regulate inflammation (*Cfb*, *Tnfa*, and *Il-6*) and cardiomyogenesis in response to hypertension-related pressure overload, β -adrenergic agonists, or myocardial infarction-induced cell injury.³⁰ Thus, *Cfb* may contribute to both cardiac inflammation and hypertrophy in response to stress, possibly through regulation of cardiomyogenic gene expression. For example, we showed complete or near complete abrogation in *Cfb*^{−/−} rats of the isoproterenol-stimulated increase in *Acta1* and *Nppb* expression seen in SHR. Further, *Nppa* expression was increased in both saline- and isoproterenol-treated *Cfb*^{−/−}. Therefore, independent of blood pressure, the lack of compensatory *Acta1* upregulation and the favourable *Acta1:Acta1* ratio³¹ indicate that the *Cfb*^{−/−} LV may be partially protected from compensatory cytoskeletal changes associated with LV dysfunction. Equally, abrogation of *Nppb* expression in the presence of isoproterenol indicates that the *Cfb*^{−/−} LV is partly protected from stress. Further, upregulation of *Nppa* in *Cfb*^{−/−} rats may, in part, contribute to the observed reduction in cardiomyocyte diameter and LV mass. Taken together, in *Cfb*^{−/−} rats, upregulation of *Nppa* and abrogation of *Acta1* expression in the presence of isoproterenol may indicate a blood pressure-independent mechanism for preserving LV function.

In addition to glucose metabolism and hypertension, we assessed the concentration of circulating lipids and Th-1 cytokines and showed reduced cholesterol and triglycerides, as well as reduced proinflammatory cytokines in *Cfb*^{−/−} rats. Some of the metabolic and immune parameters that we measured here have also been measured in a *Cfb*^{−/−} mouse, although no

cardiovascular measurements have been reported. Like the *Cfb*^{−/−} rat, the *Cfb*^{−/−} mouse lacks AP activity and has reduced Tnf α , Il-6, and Ifn- γ .^{32,33} Although having some immune similarities to the *Cfb*^{−/−} rat, *Cfb*^{−/−} mice compared with WT mice are more glucose intolerant and have higher circulating triglycerides.³⁴ The differences between these 2 models could be because of several reasons, including genetic background affecting metabolism differently, the use of high-fat diet in the mouse studies to elicit a phenotype, and the presence of 2 protein-coding *Cfb* transcripts in the mouse, whereas rats and humans have only one. On a high-fat diet, *Ldlr*^{−/−}/*Cfb*^{−/−} mice showed protection against atherosclerosis,³⁵ which is distinct from the amelioration in metabolic and cardiovascular phenotypes that we observed here. However, the 2 studies combined strongly encourage further investigation of *Cfb* as a target for protection from the development of cardiovascular disease.

Rat *Cfb* resides on chromosome 20p12, a region previously found to be important in the regulation of blood pressure, glucose homeostasis, and adiposity in SHR.^{18–21} We propose that *Cfb*, at least in SHR, plays a major part in the development of key features of MetS that are linked to 20p12. However, given that the SHR.1N congenic that covers 20p12 has a reduction of 20 mm Hg, other genes in the region may also contribute.¹⁹

The location of human *CFB* and the syntenic region to the rat gene is on human 6p21.33.¹⁸ We located 18 SNPs with genome-wide significant associations to cardiometabolic traits ≤ 1 Mb from *CFB*. Several GWAS hits in the region were associated with type 2 diabetes mellitus and components of MetS. Two SNPs, rs13196329 and rs2247056, were correlated with visceral fat, triglycerides, and *CFB* expression. Further, 1 SNP, rs805303, was significantly positively correlated with systolic and diastolic blood pressure, and hypertension, as well as with increased *CFB* expression. These results suggest that *CFB* expression associated with these SNPs may be causally linked to accumulation of visceral fat, circulating lipids, and development of hypertension in humans.

In addition to altering complement activity, *Cfb* ablation reduced proinflammatory cytokines Ifn- γ , Il-6, and Tnf α whose elevated levels are associated with hypertension, obesity, and insulin resistance.^{36,37} Further, chronic low-grade inflammation and overactivation of the innate immune system are now recognized causes of type 2 diabetes mellitus,^{4,5} with clinical trials for therapeutic targets against inflammatory pathways for the treatment of diabetes mellitus and cardiovascular disease currently underway.³⁸

Compounds that target CFB already exist, and taken together with the findings in our study, suggest that CFB has significant potential as a novel target for treatment of metabolic disease^{39,40}

This is the first study to report the widespread amelioration of metabolic and cardiovascular phenotypes through deletion of an alternative complement pathway gene in a model of MetS. *Cfb* deletion improves glucose homeostasis, adipose distribution and function, lowers blood pressure and reduces cardiac hypertrophy, protecting against LV stress. Together with our analysis of the human *CFB* region for cardiometabolic traits, we conclude that *CFB* expression and function may directly or indirectly regulate multiple metabolic and cardiovascular processes in health and disease in the rat and in humans.

Perspectives

CFB is elevated in human cohorts with type 2 diabetes mellitus and cardiovascular disease, although a causal relationship has yet to be established. We identified alterations in *Cfb* expression as a possible cause of hypertension and insulin resistance in the SHR. *Cfb* knockout rats have improved glucose homeostasis linked to favorable alterations in adipose tissue distribution and function and reduced blood pressure and LV mass suggesting new adipose tissue-intrinsic and blood pressure-independent mechanisms for SHR insulin resistance and cardiac hypertrophy. SNPs in human *CFB* are associated both with hypertension and visceral adiposity and with *CFB* gene expression, suggesting that genetic variation in *CFB* may, in part, explain the genetic associations at the human *CFB* locus. Further studies are required to establish whether overexpression of adipose tissue *Cfb* alone is the prime determinant of MetS traits. Clinical trials are presently being undertaken to test the therapeutic effects of CFB inhibitors and to investigate AP components as causal factors in human diseases related to overactivity of the innate immune system. Given the findings in this study, CFB may also be a valid therapeutic target to treat or prevent progression of human MetS.

Acknowledgments

Ultrasound imaging was performed by A.T. of Edinburgh Preclinical Imaging, University of Edinburgh. Histological processing and flow cytometry was carried out by the Shared University Research Facilities and Queen's Medical Research Institute Flow Cytometry and Cell Sorting Facility, Edinburgh. Whole genome sequencing was performed at Edinburgh Genomics Clinical Genomics, Edinburgh, United Kingdom. T.J.A. has received speaker honoraria from Illumina, Inc, and consultancy fees from AstraZeneca.

Sources of Funding

P.M.C., M.B., N.A., A.G.D., and J.M. are funded by an Advanced Grant ERC-2010-AdG_20100317 (ELABORATE; elucidation of the molecular and functional basis of disease phenotypes in the rat model) from the European Research Council awarded to T.J.A. R.N.C. and N.M.M. are funded by a Wellcome Trust New Investigator grant 100981/Z/13/Z awarded to N.M.M. S.M.P. and L.H.J.-J. are funded by Medical Research Council grants MR/N005902/1 and MR/M011542/1, respectively. Radiotelemetry equipment was funded by a Wellcome Trust Institutional Strategic Support Fund (ISSF2) award J22737 and the British Heart Foundation Centre of Research Excellence, University of Edinburgh.

Disclosures

T.J.A. has received speaker honoraria from and has research collaborations with Illumina and has received consultancy fees from AstraZeneca. The other authors report no conflicts.

References

- Motillo S, Filion K, Genest J, Joseph L, Pilote L, Poirier P, Rinfret S, Schiffrin E, Eisenberg M. The metabolic syndrome and cardiovascular risk a systematic review and meta-analysis. *J Am Coll Cardiol*. 2010;56:1113–1132. doi: 10.1016/j.jacc.2010.05.034.
- Min JL, Nicholson G, Halgrimsdottir I, et al; GIANT Consortium; MolPAGE Consortium. Coexpression network analysis in abdominal and gluteal adipose tissue reveals regulatory genetic loci for metabolic syndrome and related phenotypes. *PLoS Genet*. 2012;8:e1002505. doi: 10.1371/journal.pgen.1002505.
- Liu C, Kraja AT, Smith JA, et al; CHD Exome+ Consortium; ExomeBP Consortium; GoT2DGenes Consortium; T2D-GENES Consortium; Myocardial Infarction Genetics and CARDIoGRAM Exome Consortia; CKDGen Consortium. Meta-analysis identifies common and rare variants influencing blood pressure and overlapping with metabolic trait loci. *Nat Genet*. 2016;48:1162–1170. doi: 10.1038/ng.3660.
- Saltiel AR, Olefsky JM. Inflammatory mechanisms linking obesity and metabolic disease. *J Clin Invest*. 2017;127:1–4. doi: 10.1172/JCI92035.
- McLaughlin T, Ackerman SE, Shen L, Engleman E. Role of innate and adaptive immunity in obesity-associated metabolic disease. *J Clin Invest*. 2017;127:5–13. doi: 10.1172/JCI88876.
- Ricklin D, Hajishengallis G, Yang K, Lambris JD. Complement: a key system for immune surveillance and homeostasis. *Nat Immunol*. 2010;11:785–797. doi: 10.1038/ni.1923.
- Somani R, Richardson VR, Standeven KF, Grant PJ, Carter AM. Elevated properdin and enhanced complement activation in first-degree relatives of south asian subjects with type 2 diabetes. *Diabetes Care*. 2012;35:894–899. doi: 10.2337/dc11-1483.
- Moreno-Navarrete JM, Martinez-Barricarte R, Catalan V, Sabater M, Gomez-Ambrosi J, Ortega FJ, Ricart W, Bluhm M, Fruhbeck G, Rodriguez de Cordoba S, Fernandez-Real JM. Complement factor H is expressed in adipose tissue in association with insulin resistance. *Diabetes*. 2010;59:200–209. doi: 10.2337/db09-0700.
- Hertle E, Arts IC, van der Kallen CJ, Feskens EJ, Schalkwijk CG, Stehouwer CD, van Greevenbroek MM. The alternative complement pathway is longitudinally associated with adverse cardiovascular outcomes. The CODAM study. *Thromb Haemost*. 2016;115:446–457. doi: 10.1160/TH15-05-0439.
- Donahue MP, Rose K, Hochstrasser D, Vonderscher J, Grass P, Chibout SD, Nelson CL, Sinnaeve P, Goldschmidt-Clermont PJ, Granger CB. Discovery of proteins related to coronary artery disease using industrial-scale proteomics analysis of pooled plasma. *Am Heart J*. 2006;152:478–485. doi: 10.1016/j.ahj.2006.03.007.
- Rao RH. Insulin resistance in spontaneously hypertensive rats. Difference in interpretation based on insulin infusion rate or on plasma insulin in glucose clamp studies. *Diabetes*. 1993;42:1364–1371.
- Aitman TJ, Glazier AM, Wallace CA, et al. Identification of Cd36 (fat) as an insulin-resistance gene causing defective fatty acid and glucose metabolism in hypertensive rats. *Nat Genet*. 1999;21:76–83. doi: 10.1038/5013.
- Pravenec M, Zidek V, Simakova M, et al. Genetics of CD36 and the clustering of multiple cardiovascular risk factors in spontaneous hypertension. *J Clin Invest*. 1999;103:1651–1657. doi: 10.1172/JCI6691.
- Aitman TJ, Critser JK, Cuppen E, et al. Progress and prospects in rat genetics: a community view. *Nat Genet*. 2008;40:516–522. doi: 10.1038/ng.147.
- Pietka TA, Schappe T, Conte C, Fabbrini E, Patterson BW, Klein S, Abumrad NA, Love-Gregory L. Adipose and muscle tissue profile of CD36 transcripts in obese subjects highlights the role of CD36 in fatty acid homeostasis and insulin resistance. *Diabetes Care*. 2014;37:1990–1997. doi: 10.2337/dc13-2835.
- McDermott-Roe C, Ye J, Ahmed R, et al. Endonuclease G is a novel determinant of cardiac hypertrophy and mitochondrial function. *Nature*. 2011;478:114–118. doi: 10.1038/nature10490.
- Pravenec M, Kozich V, Krijt J, Sokolová J, Zidek V, Landa V, Mlejnek P, Šilhavý J, Šimáková M, Škop V, Trnovská J, Kazdová L, Kajiya T, Wang J, Kurtz TW. Genetic variation in renal expression of folate receptor 1 (Folr1) gene predisposes spontaneously hypertensive rats to metabolic syndrome. *Hypertension*. 2016;67:335–341. doi: 10.1161/HYPERTENSIONAHA.115.06158.
- Shimoyama M, De Pons J, Hayman GT, Lauderkind SJ, Liu W, Nigam R, Petri V, Smith JR, Tutaj M, Wang SJ, Worthey E, Dwinell M, Jacob H. The rat genome database 2015: genomic, phenotypic and environmental variations and disease. *Nucleic Acids Res*. 2015;43(Database issue):D743–D750. doi: 10.1093/nar/gku1026.

19. Pravenec M, Klír P, Kren V, Zicha J, Kunes J. An analysis of spontaneous hypertension in spontaneously hypertensive rats by means of new recombinant inbred strains. *J Hypertens*. 1989;7:217–221.
20. Bottger A, van Lith H, Kren V, Krenová D, Bílá V, Vorlíček J, Zídek V, Musilová A, Zdobinská M, Wang J, van Zutphen B, Kurtz T, Pravenec M. Quantitative trait loci influencing cholesterol and phospholipid phenotypes map to chromosomes that contain genes regulating blood pressure in the spontaneously hypertensive rat. *J Clin Invest*. 1996;98:856–862. doi: 10.1172/JCI118858.
21. Pausova Z, Sedova L, Berube J, Hamet P, Tremblay J, Dumont M, Gaudet D, Pravenec M, Kren V, Kunes J. Segment of rat chromosome 20 regulates diet-induced augmentations in adiposity, glucose intolerance, and blood pressure. *Hypertension*. 2003;41:1047–1055. doi: 10.1161/01.HYP.0000064347.49341.0B.
22. Morrissey C, Grieve IC, Heinig M, Atanur S, Petretto E, Pravenec M, Hubner N, Aitman TJ. Integrated genomic approaches to identification of candidate genes underlying metabolic and cardiovascular phenotypes in the spontaneously hypertensive rat. *Physiol Genomics*. 2011;43:1207–1218. doi: 10.1152/physiolgenomics.00210.2010.
23. Huang PL. A comprehensive definition for metabolic syndrome. *Dis Model Mech*. 2009;2:231–237. doi: 10.1242/dmm.001180.
24. Berndt J, Kovacs P, Ruschke K, Klötting N, Fasshauer M, Schön MR, Körner A, Stumvoll M, Blüher M. Fatty acid synthase gene expression in human adipose tissue: association with obesity and type 2 diabetes. *Diabetologia*. 2007;50:1472–1480. doi: 10.1007/s00125-007-0689-x.
25. Coelho M, Oliveira T, Fernandes R. Biochemistry of adipose tissue: an endocrine organ. *Arch Med Sci*. 2013;9:191–200. doi: 10.5114/aoms.2013.33181.
26. Ma K, Cabrero A, Saha P, Kojima H, Li L, Chang B, Paul A, Chan L. Increased beta-oxidation but no insulin resistance or glucose intolerance in mice lacking adiponectin. *J Biol Chem*. 2002;277:34658–34661. doi: 10.1074/jbc.C200362200.
27. Maeda N, Shimomura I, Kishida K, et al. Diet-induced insulin resistance in mice lacking adiponectin/ACRP30. *Nat Med*. 2002;8:731–737. doi: 10.1038/nm724.
28. Bassi M, do Carmo J, Hall J, da Silva A. Chronic effects of centrally administered adiponectin on appetite, metabolism and blood pressure regulation in normotensive and hypertensive rats. *Peptides*. 2012;37:1–5. doi: 10.1016/j.peptides.2012.06.013.
29. TaegtMeyer H, Sen S, Vela D. Return to the fetal gene program: a suggested metabolic link to gene expression in the heart. *Ann NY Acad Sci*. 2010;1188:191–198. doi: 10.1111/j.1749-6632.2009.05100.x.
30. Singh MV, Anderson ME. Is CaMKII a link between inflammation and hypertrophy in heart? *J Mol Med (Berl)*. 2011;89:537–543. doi: 10.1007/s00109-011-0727-5.
31. Berni R, Savi M, Bocchi L, Delucchi F, Musso E, Chaponnier C, Gabbiani G, Clement S, Stili D. Modulation of actin isoform expression before the transition from experimental compensated pressure-overload cardiac hypertrophy to decompensation. *Am J Physiol Heart Circ Physiol*. 2009;296:H1625–H1632. doi: 10.1152/ajpheart.01057.2008.
32. Matsumoto M, Fukuda W, Circolo A, Goellner J, Strauss-Schoenberger J, Wang X, Fujita S, Hidvegi T, Chaplin DD, Colten HR. Abrogation of the alternative complement pathway by targeted deletion of murine factor B. *Proc Natl Acad Sci USA*. 1997;94:8720–8725.
33. Na M, Jarneborn A, Ali A, Welin A, Magnusson M, Stokowska A, Pekna M, Jin T. Deficiency of the complement component 3 but not factor B aggravates staphylococcus aureus septic arthritis in mice. *Infect Immun*. 2016;84:930–939. doi: 10.1128/IAI.01520-15.
34. Pagliarunga S, Fiset A, Yan Y, Deshaies Y, Brouillette JF, Pekna M, Cianflone K. Acylation-stimulating protein deficiency and altered adipose tissue in alternative complement pathway knockout mice. *Am J Physiol Endocrinol Metab*. 2008;294:E521–E529. doi: 10.1152/ajpendo.00590.2007.
35. Malik TH, Cortini A, Carassiti D, Boyle JJ, Haskard DO, Botto M. The alternative pathway is critical for pathogenic complement activation in endotoxin- and diet-induced atherosclerosis in low-density lipoprotein receptor-deficient mice. *Circulation*. 2010;122:1948–1956. doi: 10.1161/CIRCULATIONAHA.110.981365.
36. Lee BC, Lee J. Cellular and molecular players in adipose tissue inflammation in the development of obesity-induced insulin resistance. *Biochim Biophys Acta*. 2014;1842:446–462. doi: 10.1016/j.bbdis.2013.05.017.
37. Idris-Khodja N, Mian MO, Paradis P, Schiffrin EL. Dual opposing roles of adaptive immunity in hypertension. *Eur Heart J*. 2014;35:1238–1244. doi: 10.1093/eurheartj/ehu119.
38. Goldfine AB, Shoelson SE. Therapeutic approaches targeting inflammation for diabetes and associated cardiovascular risk. *J Clin Invest*. 2017;127:83–93. doi: 10.1172/JCI88884.
39. Kadam AP, Sahu A. Identification of complin, a novel complement inhibitor that targets complement proteins factor B and C2. *J Immunol*. 2010;184:7116–7124. doi: 10.4049/jimmunol.1000200.
40. Grossman TR, Hettrick LA, Johnson RB, Hung G, Peralta R, Watt A, Henry SP, Adamson P, Monia BP, McCaleb ML. Inhibition of the alternative complement pathway by antisense oligonucleotides targeting complement factor B improves lupus nephritis in mice. *Immunobiology*. 2016;221:701–708. doi: 10.1016/j.imbio.2015.08.001.

Novelty and Significance

What Is New?

- Cfb—an innate immune component—is a determinant of adipose tissue distribution, glucose homeostasis, blood pressure, and LV mass in the SHR.

What Is Relevant?

- Cfb, directly or indirectly, drives novel adipose tissue-intrinsic and blood pressure-independent mechanisms for SHR insulin resistance, hypertension, and cardiac hypertrophy. SNPs associated with cardiometabolic traits and *CFB* gene expression, suggest variation in *CFB* may, in part, underlie these traits in humans.

Summary

Metabolic and cardiovascular components of MetS are improved by ablation of the *Cfb* gene in SHR. At the human *CFB* locus, 3 SNPs are significantly associated with visceral adiposity, hypertension, and *CFB* gene expression.

Complement Factor B Is a Determinant of Both Metabolic and Cardiovascular Features of Metabolic Syndrome

Philip M. Coan, Marjorie Barrier, Neza Alfazema, Roderick N. Carter, Sophie Marion de Procé, Xaquín C. Dopico, Ana Garcia Diaz, Adrian Thomson, Lucy H. Jackson-Jones, Ben Moyon, Zoe Webster, David Ross, Julie Moss, Mark J. Arends, Nicholas M. Morton and Timothy J. Aitman

Hypertension. published online July 24, 2017;

Hypertension is published by the American Heart Association, 7272 Greenville Avenue, Dallas, TX 75231

Copyright © 2017 American Heart Association, Inc. All rights reserved.

Print ISSN: 0194-911X. Online ISSN: 1524-4563

The online version of this article, along with updated information and services, is located on the World Wide Web at:

<http://hyper.ahajournals.org/content/early/2017/07/24/HYPERTENSIONAHA.117.09242>

Free via Open Access

Data Supplement (unedited) at:

<http://hyper.ahajournals.org/content/suppl/2017/07/24/HYPERTENSIONAHA.117.09242.DC1>

Permissions: Requests for permissions to reproduce figures, tables, or portions of articles originally published in *Hypertension* can be obtained via RightsLink, a service of the Copyright Clearance Center, not the Editorial Office. Once the online version of the published article for which permission is being requested is located, click Request Permissions in the middle column of the Web page under Services. Further information about this process is available in the [Permissions and Rights Question and Answer](#) document.

Reprints: Information about reprints can be found online at:

<http://www.lww.com/reprints>

Subscriptions: Information about subscribing to *Hypertension* is online at:

<http://hyper.ahajournals.org/subscriptions/>

COMPLEMENT FACTOR B IS A DETERMINANT OF BOTH METABOLIC AND CARDIOVASCULAR FEATURES OF METABOLIC SYNDROME

Short title: complement factor b knockout rat

Philip M. Coan^{1,2}, Marjorie Barrier*^{1,2}, Neza Alfazema*^{1,2}, Roderick N. Carter², Sophie Marion de Procé¹, Xaquín C. Dopico^{1,6}, Ana Garcia Diaz³, Adrian Thomson², Lucy H. Jackson-Jones², Ben Moyon⁴, Zoe Webster⁴, David Ross¹, Julie Moss¹, Mark J. Arends⁵, Nicholas M. Morton², Timothy J. Aitman^{1,2,3}.

¹ Centre for Genomic and Experimental Medicine, MRC Institute for Genetics and Molecular Medicine, Edinburgh, EH4 2XU, UK.

² University/British Heart Foundation Centre for Cardiovascular Science, Queen's Medical Research Institute, University of Edinburgh, EH16 4TJ, UK.

³ Department of Medicine, Imperial College London, London, SW7 2AZ, UK.

⁴ Embryonic Stem Cell and Transgenics Facility, MRC Clinical Sciences Centre, Imperial College London, London W12 0NN, UK.

⁵ Division of Pathology & Centre for Comparative Pathology, Edinburgh Cancer Research UK Cancer Centre, Institute of Genetics & Molecular Medicine, Edinburgh, EH4 2XR, UK.

⁶ Royal (Dick) School of Veterinary Studies, University of Edinburgh, EH25 9RG, UK.

*Equal contribution

Corresponding author:

Dr Philip M. Coan, Centre for Genomic and Experimental Medicine, MRC Institute for Genetics and Molecular Medicine, Edinburgh, EH4 2XU, UK.

+44 (0) 131 242 6690

p.m.coan.02@cantab.net

Supplemental Methods

Rats

Cfb^{-/-} rats were generated on an SHR/NCrl background (Charles River, Margate, UK), by microinjecting ZFN mRNA (Sigma), targeted to exon 6 of *Cfb* (target sequence: CCCCTCGGGCTCCATGaataTACATGGTGCTGGATG), into one-cell stage SHR/NCrl embryos that were implanted into pseudopregnant rats. Heterozygous progeny, from a founder harboring a 19 bp deletion in *Cfb*, were intercrossed to generate homozygous knockout rats. A search for off-target events was conducted by whole genome sequencing and analysed as described previously, confirmed the 19 bp deletion^{1,2}. Six additional putative variants, analysed by Sanger Sequencing, were determined to be false positives (Table S1). Rats were housed in open cages with free access to food and water. All procedures were carried out in accordance with UK Home Office regulations.

Serum analysis

Following an overnight fast, serum was extracted from whole blood exsanguinated under terminal isofluorane anaesthesia (n = 6 per group). Serum lipids were analysed by the Veterinary Pathology Laboratory, Edinburgh. In-house ELISAs were used to determine: serum Alternative complement (AP) activity (Hycult Biotech), leptin and total adiponectin (Merck Millipore), and high-molecular-weight (HMW) adiponectin and aldosterone (AMS Biotech). Serum Th1 cytokine concentrations were quantified using the LEGENDplex Rat Th1 Panel (6-plex) kit (BioLegend) and BD Accuri™ C6 Flow Cytometer (BD Biosciences). Those cytokines reported undetectable, were below the sensitivity of the assay.

Adipocyte morphometry

Epididymal fat pads were weighed, cut into five equal pieces, and processed for paraffin wax embedding (n = 6 rats per group). A random image was taken from one 4 µm thick H&E stained section per piece at 20x magnification to estimate mean adipocyte volume³: a line grid was superimposed on to each image and point sampled intercept lengths (PSI) measured between two points on the cell membrane. One hundred PSI were measured per pad and adjusted for shrinkage⁴. Fat pad weight was converted to volume according to Farvid *et al*⁵, which was then divided by mean adipocyte volume to estimate volume-weighted adipocyte number.

Glucose homeostasis

Oral glucose tolerance (OGTT) (n = 10 per group) and intravenous insulin tolerance tests (IVITT) (n = 7 per group) were performed as described^{6,7}. Glucose clearance (K_{ITT}) was calculated as described⁸.

Adipocyte metabolic rate

Isolated primary rat adipocytes (n = 6 rats per group) in Kreb's buffer (118 mM NaCl, 1.2 mM MgSO₄, 15 mM NaPO₄, 1.265 mM CaCl₂, 5.56 mM Glucose, 1% BSA) were adhered to Matrigel (Corning) coated Seahorse plates (Agilent), washed with XF-DMEM (Agilent, supplemented with 1 mM Pyruvate and 10 mM Glucose, pH 7.4), and incubated (37°C, without CO₂, 15 min). A mitochondrial stress test was performed as described previously⁹ in an XFe24 Seahorse Bioanalyser (Agilent) and oxygen consumption rate data calculated according to the manufacturer's instructions (Agilent Technologies LDA UK, Cheshire, UK).

Telemetry

Blood pressure transmitters were implanted, using isoflurane anaesthesia, according to manufacturer's instructions (HD-S10, Data Sciences International). Following surgical recovery (>7 days), blood pressure, temperature and activity were recorded for 72 h (5 min/h) (n = 8-9 per group), before subcutaneous implantation of osmotic pumps, under brief isoflurane anaesthesia, (1003D, Azlet) containing either isoproterenol (1.2 mg/kg/h) or saline (n = 4-5 per group), and further data collected for 72 h.

Echocardiography

In vivo ultrasound echocardiography was performed by using a Vevo 770 ultrasound biomicroscope (Visualsonics) with a RMV710B 25 MHz center frequency transducer in 7 week-old male rats. Briefly, isoflurane anesthetized rats were placed on a thermostatically controlled ECG monitoring table and maintained at 37°C. Parasternal long axis (PLAX) ECG-Gated Kilohertz Visualisation (EKV) B mode and M-mode views of the left ventricle (LV) were acquired. LV end-systolic and end-diastolic areas were measured by tracing the endocardial border using Vevo Analysis Software (Visualsonics) in order to calculate ejection fraction (EF) from the PLAX EKV B mode view and fractional shortening from the M-mode view.

Cardiomyocyte diameter

Left ventricle mean cardiomyocyte diameter was determined as described previously¹⁰ using images taken by QImaging Micropublisher 3.3RTV camera (QImaging) attached to an Olympus BX51 microscope (Olympus) and measured using the STEPanizer program (n = 8 per group).

Gene expression

RNA was extracted from fat depots (subcutaneous (SAT), epididymal (EAT) and brown fat (BAT)) (n = 6 per group) and left ventricle (LV) (n = 4-5 per group) for qPCR, as described previously⁸. Primer sequences are listed in Table S2. *Actb* was used as a reference gene for adipose transcripts and LV transcripts. LV transcripts from telemetric studies were normalised to *Hprt*, due to effects of isoproterenol on *Actb* expression. Ct values were compared using the $2^{-\Delta\Delta C_t}$ method.

In silico analysis of the CFB locus

Single-nucleotide polymorphisms (SNPs) associated with cardio-metabolic traits related to type 2 diabetes and MetS residing ≤ 1 Mb from human *CFB* (Table S3) were identified by mining the NHGRI GWAS catalog¹¹. Proxy SNPs, based on linkage disequilibrium were determined using SNAP (<https://archive.broadinstitute.org/mpg/snap/ldsearchpw.php>) with the 1000 genomes Pilot 1 and HapMap (release 21 and 22) databases using default parameters (0.8 r^2 threshold, 500nt distance). GWAS and proxy SNP locations (280 in total) were converted to hg19 coordinates using dbSNP¹² and the UCSC Liftover tool¹³. Associations between SNPs and *cis*-regulated expression quantitative trait loci (*cis*-eQTLs) ≤ 1 Mb from *CFB* transcription start site (TSS) were determined from tissue data files (adipose subcutaneous, artery tibial, adipose visceral omentum, artery aorta, heart atrial appendage, heart left ventricle, pancreas, artery coronary, and liver) for SNP-gene association pairs downloaded from the GTex portal

(<http://www.gtexportal.org/home/>). False discovery rate (FDR) was determined in R according to the Benjamini-Hochberg approach (<https://www.r-project.org>).

References

1. Atanur SS, Diaz AG, Maratou K, *et al.* Genome sequencing reveals loci under artificial selection that underlie disease phenotypes in the laboratory rat. *Cell*. 2013;154:691-703.
2. Van der Auwera GA, Carneiro MO, Hartl C, *et al.* From fastq data to high confidence variant calls: The genome analysis toolkit best practices pipeline. *Curr Protoc Bioinformatics*. 2013;43:11 10 11-33.
3. Tschanz SA, Burri PH, Weibel ER. A simple tool for stereological assessment of digital images: The stepanizer. *J Microsc*. 2011;243:47-59
4. Gundersen HJ, Jensen EB. Stereological estimation of the volume-weighted mean volume of arbitrary particles observed on random sections. *J Microsc*. 1985;138:127-142.
5. Farvid MS, Ng TW, Chan DC, Barrett PH, Watts GF. Association of adiponectin and resistin with adipose tissue compartments, insulin resistance and dyslipidaemia. *Diabetes Obes Metab*. 2005;7:406-413
6. Pravenec M, Landa V, Zidek V, Musilova A, Kazdova L, Qi N, Wang J, St Lezin E, Kurtz TW. Transgenic expression of cd36 in the spontaneously hypertensive rat is associated with amelioration of metabolic disturbances but has no effect on hypertension. *Physiol Res*. 2003;52:681-688.
7. Conde SV, Nunes da Silva T, Gonzalez C, Mota Carmo M, Monteiro EC, Guarino MP. Chronic caffeine intake decreases circulating catecholamines and prevents diet-induced insulin resistance and hypertension in rats. *Br J Nutr*. 2012;107:86-95.
8. Coan PM, Hummel O, Diaz AI, Barrier M, Alfazema N, Norsworthy PJ, Pravenec M, Petretto E, Huebner N, Aitman TJ. Genetic, physiological and comparative genomic studies of hypertension and insulin resistance in the spontaneously hypertensive rat. *Dis Model Mech*. 2017;10.1242/dmm.026716.
9. Bugge A, Dib L, Collins S. Measuring respiratory activity of adipocytes and adipose tissues in real time. *Methods Enzymol*. 2014;538:233-247
10. Zhao XY, Li L, Zhang JY, Liu GQ, Chen YL, Yang PL, Liu RY. Atorvastatin prevents left ventricular remodeling in spontaneously hypertensive rats. *Int Heart J*. 2010;51:426-431.
11. Welter D, MacArthur J, Morales J, Burdett T, Hall P, Junkins H, Klemm A, Flicek P, Manolio T, Hindorff L, Parkinson H. The nhgri gwas catalog, a curated resource of snp-trait associations. *Nucleic Acids Res*. 2014;42:D1001-D1006.
12. Sherry S, Ward M, Kholodov M, Baker J, Phan L, Smigielski E, Sirotkin K. Dbsnp: The ncbi database of genetic variation. *Nucleic Acids Res*. 2001;29:308-311.
13. Kent W, Sugnet C, Furey T, Roskin K, Pringle T, Zahler A, Haussler D. The human genome browser at ucsc. *Genome Res*. 2002;12:996-1006.

Supplementary Tables

Table S1. Putative ZFN off-target events that were found to be false positives

Gene name	Off-target position	Rnor_6.0	SHR/NCrI (Illumina)	<i>Cfb</i> ^{-/-} (Illumina)	SHR/NCrI (Sanger)	<i>Cfb</i> ^{-/-} (Sanger)
<i>Grb2</i>	1:98046688	GCCC	GC/GC	G/GC	GCCC	GCCC
<i>Abhd17c</i>	1:146289241	C	C/C	C/G	C	C
<i>AABR07051532.1</i>	3:16440449-749	C	G/G	G/T	C	C
<i>AABR07065498.1</i>	6:132175624	A	ACCCCC/ ACCCCC	ACCCC/ ACCCCC	A	A
<i>AABR07065768.3</i>	6:140407070	T	T/C	G/C	T	T
<i>Ppidl1</i>	9:121457023-68	C	C/C	C/T	C	C

Table S2. Primer sequences used for quantitative real-time PCR analysis

Gene	Forward	Reverse
<i>Acol</i>	TCAGATAAAGCTGGACACCGGG	CCTACTGGGCCATCTTTTCGGAT
<i>Actb</i>	ATGTACCCAGGCATTGCTGAC	GAGTACTTGCGCTCAGGAGGA
<i>Actc1</i>	CAAAGCACGCCTACAGATCCCA	GAAGACAGCTCTGGGAGCATCA
<i>Adipoq</i>	CTCCACCCAAGGAAACTTGTGC	TTAGGACCAAGAACACCTGCGT
<i>Agt</i>	GCTGGAGCTAAAGGACACACAG	AAAGGGGTGGATGTATACGCGG
<i>Camk2d</i>	AGTGAGGCTGATGCCAGTCATT	CAGGTCCCTGTGAACTATGCCA
<i>Cfb</i>	AGTAGAGATCAAAGGCGGCTCC	TTCGAGTCTGCACAGGGTATGG
<i>Cfb (ZFN)</i>	AGGTTGAGCAGGAAGCTCAG	AGGACTCGGACCCAGAGAAT
<i>Cpt1</i>	CTGAGACAGACTCACACCGCTT	GTTTTCCCTCCGTGTGGCTCAG
<i>Fasn</i>	TTGTGGACGGAGGTATCAACCC	CCATGCTGTAGCCCAGAAGAGT
<i>Hprt1</i>	TCAGTCCCAGCGTCGTGATTAG	TCGAGCAAGTCTTTCAGTCCTGT
<i>Lep</i>	CAGCAGCTGCAAGGTCCAAGA	TAGGACCAAAGCCACAGGAACC
<i>Myh6</i>	ACACCAACCTGTCCAAGTTCC	ATCGTGCATTTTCTGCTTGGCG
<i>Myh7</i>	CAACCTGTCCAAGTTCCGCAAG	ACTCTTCATTCAGGCCCTTGGC
<i>Nppa</i>	ATTTCAAGAACCTGCTAGACCACC	GCACCTCAGAGAGGGAGCTAAG
<i>Nppb</i>	ACAATCCACGATGCAGAAGCTG	GAAGGCGCTGTCTTGAGACCTA
<i>Pgcl1a</i>	TTGACTGGCGTCATTCAGGAGC	CCAGGGCAGCACACTCTATGT
<i>Renin</i>	GATCACCATGAAGGGGGTCTCT	GATCAACTGCAGGGAGCTGGTA
<i>Slc2a4</i>	TTTGCACACCACTTCCGAAGGC	GGTCCCCATCTTCAGAGCCGAT
<i>Ucp1</i>	ACATACTGGCAGATGACGTCCC	GCTGGGTACACTTGGGTACTGT

Table S3. Trait terms from the NHGRI-EBI GWAS catalog that were used to identify SNPs associated with cardiometabolic traits in the *CFB* locus

NHGRI-EBI genome-wide association cardio-metabolic trait
Basal_metabolic_rate
Blood_pressure
Blood_pressure_(age_interaction)
Blood_pressure_(anthropometric_measures_interaction)
Blood_pressure_(smoking_interaction)
Cardiac_hypertrophy
Cardiovascular_disease_in_hypertension_(ACE_inhibitor_interaction)
Cardiovascular_disease_in_hypertension_(calcium_channel_blocker_interaction)
Cardiovascular_disease_risk_factors
Cardiovascular_heart_disease_in_diabetics
Cholesterol
Cholesterol_and_Triglycerides
Cholesterol,_total
Coronary_heart_disease
Coronary_heart_disease_event_reduction_in_response_to_statin_therapy_(interaction)
Diabetes_related_insulin_traits
Diastolic_blood_pressure
Diastolic_blood_pressure_(alcohol_consumption_interaction)
Fasting_glucose-related_traits
Fasting_glucose-related_traits_(interaction_with_BMI)
Fasting_insulin_(interaction)
Fasting_insulin-related_traits
Fasting_insulin-related_traits_(interaction_with_BMI)
Fasting_plasma_glucose
Fasting_plasma_glucose_(childhood)
Glucose_homeostasis_traits
Glycemic_traits
HDL_cholesterol
HDL_Cholesterol_-_Triglycerides_(HDL-C-TG)
Hypertension
Insulin_resistance/response
LDL_cholesterol
Lipoprotein_(a)_-_cholesterol_levels
Lipoprotein_(a)_levels
Metabolic_syndrome
Metabolic_traits
Systolic_blood_pressure
Systolic_blood_pressure_(alcohol_consumption_interaction)
Systolic_blood_pressure_in_sickle_cell_anemia
Triglycerides

Triglycerides-Blood_Pressure_(TG-BP)
Two-hour_glucose_challenge
Type_2_diabetes
Type_2_diabetes_(dietary_heme_iron_intake_interaction)
Type_2_diabetes_(young_onset)_and_obesity
Type_2_diabetes_and_gout
Type_2_diabetes_and_other_traits
Type_2_diabetes_nephropathy
Visceral_adipose_tissue
Visceral_adipose_tissue_adjusted_for_BMI
Visceral_adipose_tissue/subcutaneous_adipose_tissue_ratio
Visceral_fat

Table S4. Serum analytes

Analyte	SHR	<i>Cfb</i>^{-/-}
Cholesterol (mM)	1.62 ± 0.05	1.26 ± 0.06***
Triglyceride (mM)	0.28 ± 0.01	0.24 ± 0.02**
Adiponectin (total) (ng/mL)	38.3 ± 2.8	43.4 ± 2.6
Adiponectin (HMW*) (ng/mL)	3.81 ± 0.14	2.36 ± 0.05***
Leptin (ng/mL)	0.95 ± 0.08	0.95 ± 0.05
Aldosterone (ng/mL)	272 ± 14	150 ± 6***
IL-2 (pg/mL)	undetected	undetected
IL-6 (pg/mL)	108.7 ± 6.4	undetected
IL-10 (pg/mL)	182.2 ± 24.6	45.9 ± 17.9*
GM-CSF [†] (pg/mL)	19.25 ± 4.9	10.5 ± 2.2
IFN-γ (pg/mL)	18.2 ± 1.1	7.12 ± 0.3***
TNFα (pg/mL)	8.05 ± 1.98	undetected

Results are mean ± SEM; **P* < 0.05, ***P* < 0.005, ****P* < 0.0001.

*HMW, high molecular weight.

[†]GM-CSF, granulocyte macrophage colony-stimulating factor.

Table S5. Left ventricle echocardiographic measurements at 7 weeks of age

Parameter	SHR	<i>Cfb</i>^{-/-}
LV* Mass; d (mg)	646 ± 29	542 ± 43
LV (mg/kg)	4500 ± 154	3649 ± 268*
Endocardial Volume; d [†] (μL)	251 ± 14	248 ± 10
Endocardial Volume; s [‡] (μL)	85 ± 9	64 ± 4
Endocardial Area Change (mm ²)	29.1 ± 1.5	33.6 ± 1.8
LV wall thickness; d (mm)	1.24 ± 0.05	1.08 ± 0.06
Heart Rate (beats/min)	324 ± 6	315 ± 7
Endocardial Stroke Volume (μL)	165 ± 10	183 ± 9
Ejection fraction (%)	66.2 ± 2.3	73.9 ± 1.7*
Fractional area change (%)	47.0 ± 1.8	54.8 ± 1.9**
Fractional shortening (%)	36.1 ± 0.6	43.4 ± 1.0**
Cardiac output (mL/min)	53.9 ± 3.5	57.6 ± 2.5

Results are mean ± SEM; **P* < 0.05, ***P* < 0.005, ****P* < 0.0001.

*left ventricle.

[†]d, diastole.

[‡]s, systole.

Table S6. NHGRI-EBI cardio-metabolic GWAS hits located at the *CFB* locus

Disease/trait	Strongest SNP/ risk allele	Chromosome position	Distance from <i>Cfb</i> (Mb)
Type 2 diabetes	rs3132524-G	31168937	0.775
Coronary heart disease	rs3869109-G	31216419	0.728
LDL cholesterol, total cholesterol	rs9357121	31272702	0.671
Triglycerides	rs2247056-T	31297713	0.646
SBP, DBP	rs9266359-C	31364962	0.579
Type 2 diabetes	rs2244020-G	31379674	0.564
Visceral fat adjusted for BMI	rs12175489-A	31409810	0.534
Metabolic syndrome	rs3099844-A	31481199	0.463
SBP, DBP, Hypertension	rs805303-G	31648589	0.296
SBP, DBP, Hypertension	rs2021783-C	32077074	0.126
Triglycerides	rs419132-G	32243022	0.292
Visceral fat	rs13196329-C	32357594	0.407
Coronary heart disease	rs9268402-G	32373576	0.423
Cholesterol, total	rs3177928-A	32444658	0.494
Cholesterol, total	rs114067101-G	32490183	0.539
HDL cholesterol	rs116569761	32680379	0.729
Coronary heart disease	rs11752643-T	32701596	0.751
Type 2 diabetes	rs3916765-A	32717773	0.767

Table S7. GTex *cis*-eQTLs associated with *CFB* expression

SNP Id	P-value	Effect size	Tissue	Chromosome position (Hg38)	Distance from TSS*
rs115056371	0.000084	0.17	Adipose_Subcutaneous	31238942	-706731
chr6_32630981_D	0.000051	0.18	Adipose_Subcutaneous	32663204	717531
rs9274179	0.000054	0.18	Adipose_Subcutaneous	32662687	717014
rs28746813	0.000065	0.18	Adipose_Subcutaneous	32665453	719780
chr6_32656068_I	0.000072	0.18	Adipose_Subcutaneous	32688291	742618
rs28746811	0.000076	0.18	Adipose_Subcutaneous	32665420	719747
rs28746814	0.000085	0.18	Adipose_Subcutaneous	32665470	719797
rs116066079	0.0001	0.18	Adipose_Subcutaneous	32712646	766973
rs114682366	0.0001	0.18	Adipose_Subcutaneous	32712664	766991
rs28724263	0.000023	0.19	Adipose_Subcutaneous	32664152	718479
rs114830099	0.000028	0.19	Adipose_Subcutaneous	32742444	796771
rs114515571	0.000041	0.19	Adipose_Subcutaneous	32713384	767711
rs114227315	0.000041	0.19	Adipose_Subcutaneous	32712602	766929
rs9274657	0.0000045	0.2	Adipose_Subcutaneous	32668587	722914
rs9274659	0.0000045	0.2	Adipose_Subcutaneous	32668608	722935
chr6_32656067_I	0.000021	0.2	Adipose_Subcutaneous	32688290	742617
rs9274209	0.000038	0.2	Adipose_Subcutaneous	32663043	717370
rs28746806	0.000043	0.2	Adipose_Subcutaneous	32665288	719615
rs28746832	0.000005	0.21	Adipose_Subcutaneous	32666039	720366
chr6_32632717	0.000049	0.22	Adipose_Subcutaneous	32664940	719267
rs9274227	0.000059	0.22	Adipose_Subcutaneous	32663365	717692
rs191863247	0.0000039	0.27	Adipose_Subcutaneous	32487582	541909

chr6_32632878_I	0.000042	0.28	Adipose_Subcutaneous	32665101	719428
chr6_32627913_D	0.000056	0.39	Adipose_Subcutaneous	32660136	714463
rs60302302	0.0000064	0.41	Adipose_Subcutaneous	32515926	570253
rs181165562	0.000075	0.41	Adipose_Subcutaneous	32386129	440456
rs76846904	0.000015	0.78	Adipose_Subcutaneous	32532140	586467
rs76415507	0.000009	-0.4	Artery_Aorta	32524812	579139
rs143726520	0.0000044	-0.36	Artery_Aorta	32520080	574407
rs114624824	0.000013	-0.34	Artery_Aorta	32524743	579070
rs74655967	0.000013	-0.34	Artery_Aorta	32524691	579018
rs115623335	0.0000036	-0.33	Artery_Aorta	32564801	619128
rs76851429	0.000041	-0.33	Artery_Aorta	32524591	578918
rs116640755	0.00002	-0.32	Artery_Aorta	32564779	619106
rs80237386	0.000027	-0.32	Artery_Aorta	32524716	579043
rs75906455	0.00003	-0.32	Artery_Aorta	32524742	579069
rs77159841	0.000038	-0.32	Artery_Aorta	32524733	579060
rs72492345	0.000049	-0.32	Artery_Aorta	32564838	619165
rs146763062	0.000027	-0.31	Artery_Aorta	32523894	578221
rs115814063	0.000039	-0.31	Artery_Aorta	32524316	578643
chr6_32551762_D	0.000062	-0.31	Artery_Aorta	32583985	638312
chr6_32490131_D	0.000065	-0.31	Artery_Aorta	32522354	576681
rs114553448	0.000083	-0.31	Artery_Aorta	32569362	623689
rs115918114	0.00005	-0.3	Artery_Aorta	32524524	578851
rs79949014	0.000086	-0.3	Artery_Aorta	32524609	578936
rs142399500	0.000059	-0.29	Artery_Aorta	32521691	576018
rs141142229	0.000082	-0.29	Artery_Aorta	32524028	578355

rs114980010	0.0000041	-0.33	Artery_Tibial	31604704	-340969
rs1048709	0.000049	-0.25	Artery_Tibial	31947158	1485
			Skin_Sun_Exposed_		
rs115804811	0.0000022	-0.81	Lower_leg	32570025	624352
			Skin_Sun_Exposed_		
rs74216018	0.0000089	-0.47	Lower_leg	32524667	578994
			Skin_Sun_Exposed_		
rs34382076	0.00001	-0.44	Lower_leg	32581548	635875
			Skin_Sun_Exposed_		
rs79606458	0.000045	-0.28	Lower_leg	32522036	576363

*TSS, transcription start site

Table S8. Genes residing in the 1 MB region upstream/downstream the *CFB* transcription start site

Gene stable ID	Gene Start (bp)	Gene End (bp)	Gene name
ENSG00000233529	30945979	30954862	HCG21
ENSG00000275906	30961403	30962396	XXbac-BPG118E17.10
ENSG00000204544	30983718	30989903	MUC21
ENSG00000261272	31010474	31035402	MUC22
ENSG00000228789	31053450	31059890	HCG22
ENSG00000222895	31083010	31083109	RNU6-1133P
ENSG00000204542	31111223	31112559	C6orf15
ENSG00000204540	31114750	31140092	PSORS1C1
ENSG00000204539	31115090	31120446	CDSN
ENSG00000204538	31137536	31139350	PSORS1C2
ENSG00000238211	31140727	31140913	POLR2LP1
ENSG00000204536	31142439	31158238	CCHCR1
ENSG00000137310	31158542	31167159	TCF19
ENSG00000204531	31164337	31180731	POU5F1
ENSG00000204528	31173735	31177899	PSORS1C3
ENSG00000272501	31195200	31198037	XXbac-BPG299F13.17
ENSG00000206344	31197760	31203968	HCG27
ENSG00000271821	31200165	31201918	XXbac-BPG299F13.14
ENSG00000255726	31222913	31223093	XXbac-BPG299F13.15
ENSG00000255899	31224342	31225058	XXbac-BPG299F13.16
ENSG00000204525	31268749	31272130	HLA-C
ENSG00000234745	31269491	31357188	HLA-B
ENSG00000214892	31275572	31278754	USP8P1
ENSG00000227939	31280317	31281519	RPL3P2
ENSG00000231402	31287510	31288964	WASF5P
ENSG00000256166	31293908	31301642	XXbac-BPG248L24.13
ENSG00000229836	31307815	31308549	XXbac-BPG248L24.10
ENSG00000277402	31355224	31355316	MIR6891
ENSG00000271581	31356647	31357637	XXbac-BPG248L24.12

ENSG00000228432	31366352	31366898	DHFRP2
ENSG00000201658	31370134	31370240	RNU6-283P
ENSG00000230994	31377419	31378019	FGFR3P1
ENSG00000223702	31380411	31380839	ZDHHC20P2
ENSG00000225851	31382074	31382288	HLA-S
ENSG00000272221	31394289	31395495	XXbac-BPG181B23.7
ENSG00000204520	31399784	31415315	MICA
ENSG00000206337	31400702	31477506	HCP5
ENSG00000199332	31402152	31402250	Y_RNA
ENSG00000230174	31441667	31446973	LINC01149
ENSG00000233902	31462728	31463336	XXbac-BPG181B23.6
ENSG00000204516	31494881	31511124	MICB
ENSG00000201680	31496689	31496790	Y_RNA
ENSG00000256851	31515979	31516211	XXbac-BPG16N22.5
ENSG00000219797	31519480	31520291	PPIAP9
ENSG00000225499	31528114	31528693	RPL15P4
ENSG00000204511	31528717	31530232	MCCD1
ENSG00000198563	31530219	31542448	DDX39B
ENSG00000254870	31530219	31546608	ATP6V1G2-DDX39B
ENSG00000201785	31536374	31536449	SNORD117
ENSG00000265236	31541101	31541178	SNORD84
ENSG00000234006	31542304	31543138	DDX39B-AS1
ENSG00000213760	31544462	31548427	ATP6V1G2
ENSG00000204498	31546870	31558829	NFKBIL1
ENSG00000226979	31572054	31574324	LTA
ENSG00000232810	31575567	31578336	TNF
ENSG00000227507	31580525	31582522	LTB
ENSG00000204482	31586124	31588909	LST1
ENSG00000204475	31588895	31592985	NCR3
ENSG00000230622	31611083	31611356	UQCRHP1
ENSG00000204472	31615184	31617021	AIF1

ENSG00000204469	31620720	31637771	PRRC2A
ENSG00000200816	31623079	31623210	SNORA38
ENSG00000274494	31633787	31633858	MIR6832
ENSG00000204463	31639028	31652705	BAG6
ENSG00000204444	31652416	31658210	APOM
ENSG00000204439	31658298	31660772	C6orf47
ENSG00000227198	31658329	31660721	C6orf47-AS1
ENSG00000204438	31661229	31666283	GPANK1
ENSG00000201207	31663288	31663401	Y_RNA
ENSG00000204435	31665236	31670343	CSNK2B
ENSG00000263020	31666102	31673546	XXbac-BPG32J3.22
ENSG00000240053	31670167	31673776	LY6G5B
ENSG00000204428	31676684	31684040	LY6G5C
ENSG00000204427	31686949	31703444	ABHD16A
ENSG00000204422	31686962	31714072	XXbac-BPG32J3.20
ENSG00000266776	31701029	31701091	MIR4646
ENSG00000204424	31706885	31710595	LY6G6F
ENSG00000250641	31706904	31717918	XXbac-BPG32J3.19
ENSG00000255552	31711771	31714065	LY6G6E
ENSG00000244355	31715356	31717804	LY6G6D
ENSG00000204420	31718594	31726714	MPIG6B
ENSG00000204421	31718648	31721845	LY6G6C
ENSG00000213722	31727038	31730617	DDAH2
ENSG00000213719	31730581	31739763	CLIC1
ENSG00000204410	31739948	31762834	MSH5
ENSG00000255152	31740020	31764851	MSH5-SAPCD1
ENSG00000252743	31756951	31757053	RNU6-850P
ENSG00000228727	31762799	31764851	SAPCD1
ENSG00000235663	31764310	31765588	SAPCD1-AS1
ENSG00000204396	31765590	31777294	VWA7
ENSG00000204394	31777518	31795953	VARS

ENSG00000201555	31778817	31778905	Y_RNA
ENSG00000204392	31797396	31806984	LSM2
ENSG00000204390	31809619	31815065	HSPA1L
ENSG00000204389	31815464	31817946	HSPA1A
ENSG00000204388	31827735	31830255	HSPA1B
ENSG00000204387	31834608	31839766	C6orf48
ENSG00000201823	31835263	31835326	SNORD48
ENSG00000201754	31837076	31837142	SNORD52
ENSG00000204386	31857659	31862906	NEU1
ENSG00000204385	31863192	31879046	SLC44A4
ENSG00000204371	31879759	31897687	EHMT2
ENSG00000237080	31883761	31884204	EHMT2-AS1
ENSG00000166278	31897785	31945672	C2
ENSG00000204366	31899607	31901992	ZBTB12
ENSG00000244255	31927698	31952048	XXbac-BPG116M5.17
ENSG00000281756	31934474	31941724	C2-AS1
ENSG00000243649	31945650	31952084	CFB
ENSG00000204356	31952087	31959110	NELFE
ENSG00000284446	31956839	31956940	MIR1236
ENSG00000204351	31959080	31969755	SKIV2L
ENSG00000204348	31969810	31972292	DXO
ENSG00000204344	31971091	31982821	STK19
ENSG00000244731	31982024	32002681	C4A
ENSG00000233627	31999976	32003521	C4A-AS1
ENSG00000204338	32005636	32008451	CYP21A1P
ENSG00000248290	32008614	32012472	TNXA
ENSG00000250535	32013270	32013787	STK19B
ENSG00000224389	32014762	32035418	C4B
ENSG00000229776	32032713	32036258	C4B-AS1
ENSG00000231852	32038265	32041670	CYP21A2
ENSG00000168477	32041154	32115334	TNXB

ENSG00000252512	32078508	32078628	RNA5SP206
ENSG00000213676	32098176	32128253	ATF6B
ENSG00000204315	32128707	32130291	FKBPL
ENSG00000204314	32148359	32154373	PRRT1
ENSG00000221988	32153441	32163680	PPT2
ENSG00000258388	32153845	32171978	PPT2-EGFL8
ENSG00000241404	32164583	32168281	EGFL8
ENSG00000204310	32168212	32178096	AGPAT1
ENSG00000284469	32170030	32170116	MIR6721
ENSG00000204308	32178354	32180793	RNF5
ENSG00000277264	32179816	32179876	MIR6833
ENSG00000204305	32180968	32184324	AGER
ENSG00000273333	32184733	32185882	XXbac-BPG300A18.13
ENSG00000204304	32184741	32190186	PBX2
ENSG00000213654	32190766	32195523	GPSM3
ENSG00000204301	32194843	32224067	NOTCH4
ENSG00000277427	32255284	32350039	XXbac-BPG154L12.5
ENSG00000225914	32255711	32265838	XXbac-BPG154L12.4
ENSG00000204296	32288526	32371912	C6orf10
ENSG00000237285	32325219	32326178	HNRNPA1P2
ENSG00000223335	32352877	32352983	RNU6-603P
ENSG00000228962	32390510	32393686	HCG23
ENSG00000204290	32393963	32407128	BTNL2
ENSG00000204287	32439842	32445046	HLA-DRA
ENSG00000196301	32459821	32473500	HLA-DRB9
ENSG00000198502	32517343	32530287	HLA-DRB5
ENSG00000251916	32549940	32550090	RNU1-61P
ENSG00000229391	32552713	32560022	HLA-DRB6
ENSG00000196126	32578769	32589848	HLA-DRB1
ENSG00000196735	32628179	32647062	HLA-DQA1
ENSG00000179344	32659467	32668383	HLA-DQB1

ENSG00000223534	32659880	32660729	HLA-DQB1-AS1
ENSG00000235040	32706124	32706955	MTCO3P1
ENSG00000232080	32718005	32719170	XXbac-BPG254F23.7
ENSG00000226030	32730758	32731695	HLA-DQB3
ENSG00000237541	32741342	32747215	HLA-DQA2
ENSG00000263649	32749912	32749979	MIR3135B
ENSG00000232629	32756098	32763534	HLA-DQB2
ENSG00000241106	32812763	32817048	HLA-DOB
ENSG00000250264	32813767	32838822	XXbac-BPG246D15.9
ENSG00000204267	32821833	32838780	TAP2
ENSG00000204264	32840717	32844703	PSMB8
ENSG00000204261	32844086	32846495	PSMB8-AS1
ENSG00000240065	32844136	32859585	PSMB9
ENSG00000168394	32845209	32853978	TAP1
ENSG00000234515	32879171	32879848	PPP1R2P1
ENSG00000235301	32896416	32896490	HLA-Z
ENSG00000242574	32934629	32941070	HLA-DMB

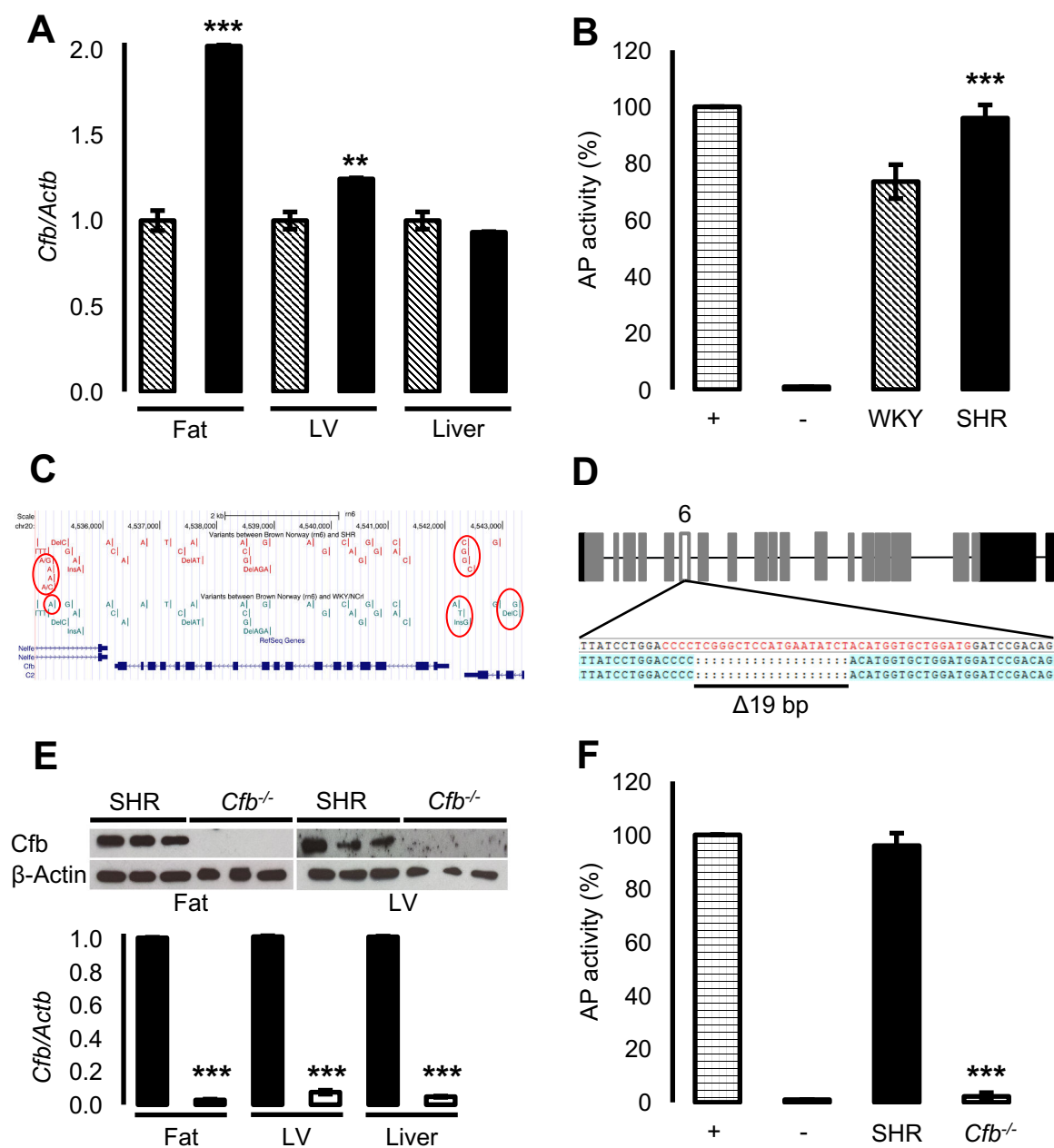


Figure S1. Generation of a complement factor b knockout rat on an SHR background. (A) qPCR analysis of *Cfb* expression epididymal (Fat), left ventricle (LV) and liver from SHR (filled bars) and WKY (striped bars). (B) Serum alternative complement (AP) activity in SHR compared to WKY (+, positive control, -, negative control). (C) Graphical representation of *Cfb* detailing unique variants in SHR (red-circled) compared to BN and WKY. (D) Diagram of the exon-intron structure of the rat *Cfb* gene indicating the 19 bp deletion generated by zinc-finger nucleases in exon 6. (E) qPCR analysis of *Cfb* and immunoblot of Cfb protein expression in epididymal adipose tissue (Fat), left ventricle (LV) and liver, showing protein and transcript ablation in *Cfb*^{-/-} tissues, SHR (black-filled bars) and *Cfb*^{-/-} (white-filled bars). (F) Serum AP complement activity in *Cfb*^{-/-} (open bar) compared to SHR (filled bar) (+, positive control, -, negative control). (n = 5-6 per group). **P* < 0.05, ***P* < 0.01, ****P* < 0.001.

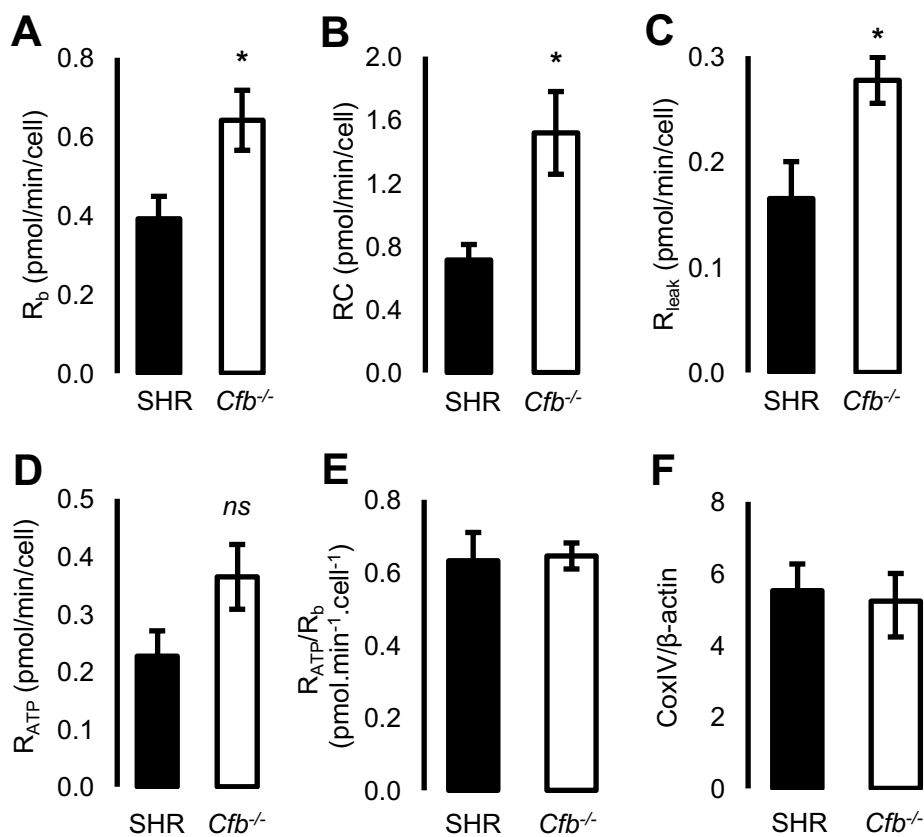


Figure S2. Oxygen consumption rate (OCR) and CoxIV abundance in isolated adipocytes from SHR and *Cfb*^{-/-} rats. (A) basal respiratory rate, (B) reserve capacity (RC), (C) leak respiration, (D) ATP-linked respiration, and (E) ATP efficiency non-respiratory oxygen consumption rate in isolated epididymal adipocytes. (F) expression of CoxIV protein abundance in epididymal fat (n = 6 per group). **P* < 0.05.

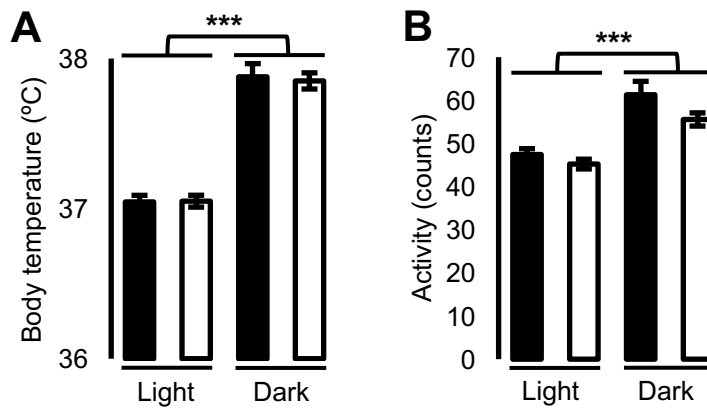


Figure S3. Telemetric measurements of (A) mean core body temperature and (B) activity (n = 8-9 per group). *Cfb*^{-/-} (open bars) compared to SHR (filled bars). Significant differences between light and dark periods ****P* < 0.001.

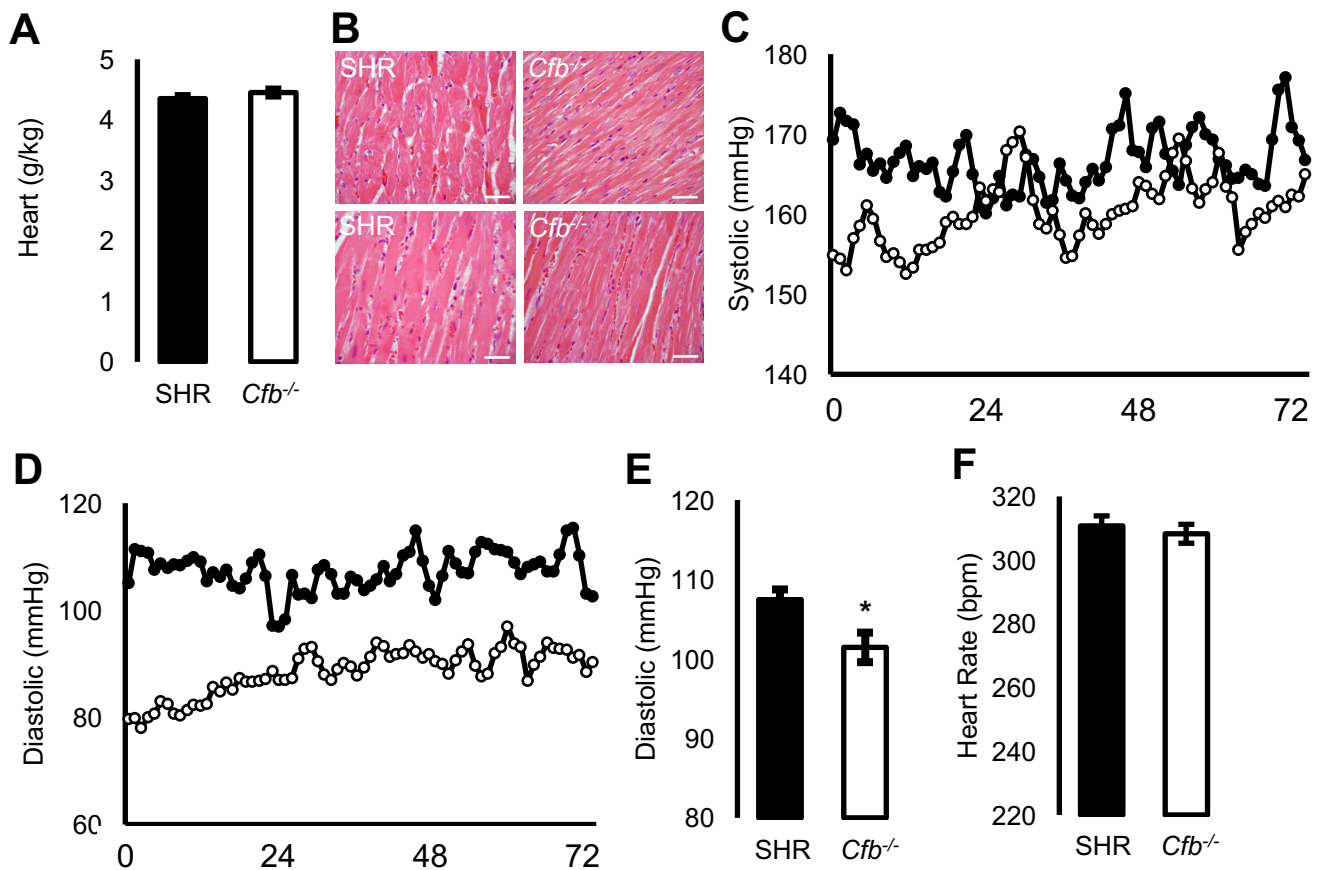


Figure S4. Baseline cardiovascular measurements. (A) Relative heart wet mass (n = 15 per group). (B) Light micrographs of representative H&E stained left ventricle sections (scale bar 10 μ m). (C) Systolic and (D) diastolic blood pressure hourly plots during 72 h (n = 8-9 per group). (E) Mean diastolic blood pressure and (G) Heart rate. * $P < 0.05$.

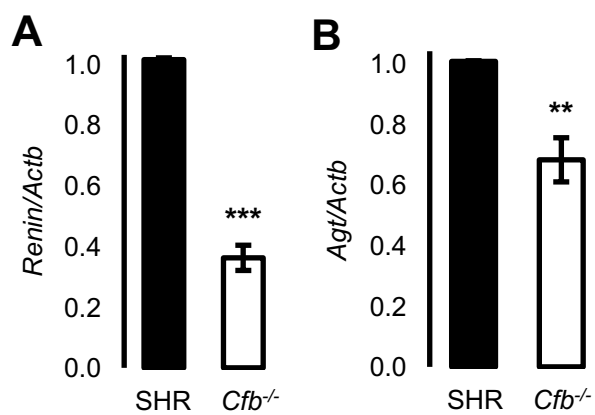


Figure S5. Gene expression of (H) renal renin and (I) hepatic angiotensinogen (n = 6 per group). ** $P < 0.01$, *** $P < 0.001$

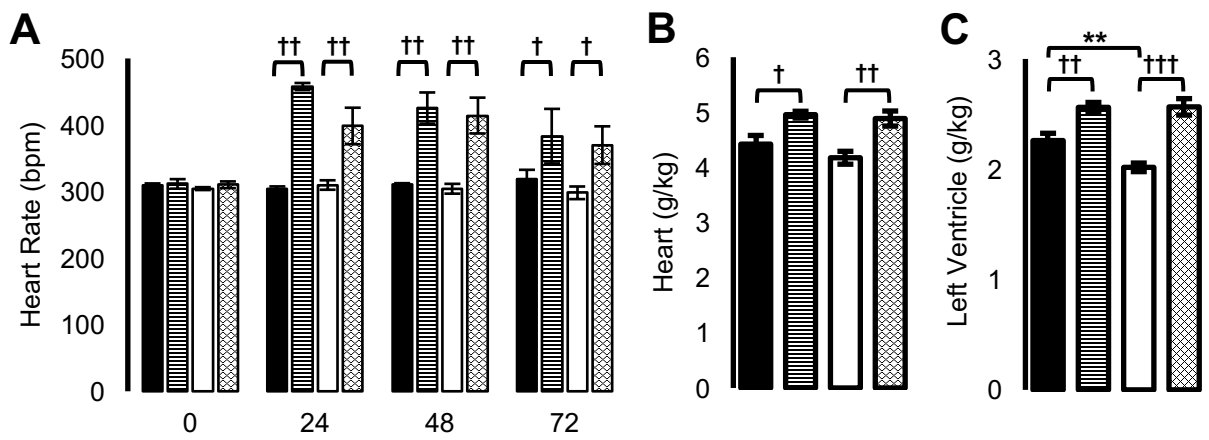


Figure. S6. Wet cardiac masses taken from rats treated with isoproterenol and saline for 72 h. (A) Heart rate, (B) relative heart and (C) left ventricle wet masses (n = 4-5 per group). Black-filled bars, SHR, saline-treated; Stripe-filled bars, SHR, isoproterenol-treated; White-filled bars, *Cfb*^{-/-}, saline-treated; Hatch-filled bars, *Cfb*^{-/-}, isoproterenol-treated. Differences in genotype ^{††}*P* < 0.01 or treatment [†]*P* < 0.05, ^{††}*P* < 0.01, ^{†††}*P* < 0.001.

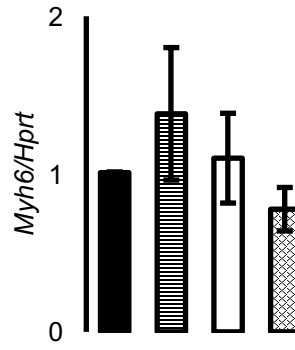


Figure S7. *Myh6* expression levels in left ventricles following 72h isoproterenol or saline treatment. Black-filled bars, SHR, saline-treated; Stripe-filled bars, SHR, isoproterenol-treated; White-filled bars, *Cfb*^{-/-}, saline-treated; Hatch-filled bars, *Cfb*^{-/-}, isoproterenol-treated.